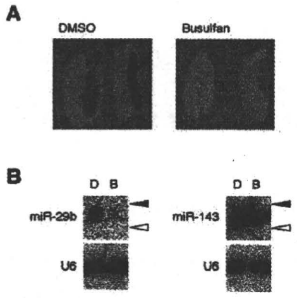

FIGURE 4. Expression of miR-29b and miR-143 in PGCs of mouse embryos at E13.5. (*A*) Male (M) and female (F) embryonic gonads were recovered at E13.5 from dams injected with DMSO or busulfan and were subjected to whole-mount in situ hybridization with a probe specific for *Oct4* mRNA. (*B*) Fractions containing small RNAs isolated from female or male gonads treated as in *A* were subjected to Northern blot analysis with probes specific for miR-29b or miR-143, respectively. The same blots were also subjected to hybridization with a probe specific for U6 RNA. (Closed and open arrowheads) The positions corresponding to 24 and 19 nt, respectively. Embryos exposed to (D) DMSO or (B) busulfan.

constructs (Fig. 5B), likely because miR-29b is expressed in NIH3T3 cells (data not shown). Furthermore, the luciferase activities of the wild-type constructs for *Dnmt3a* or *Dnmt3b* were reduced by cotransfection with miR-29b, whereas those of the mutant constructs were not (Fig. 5B). These results thus suggested that both genes may be targets of miR-29b in mouse.

DISCUSSION

We have determined the miRNA expression profiles of male and female embryonic mouse gonads at E13.5. Given that most conventional methods for cloning of miRNAs require >100 μg of total RNA (Lagos-Quintana et al. 2002), it would have been difficult to profile miRNA expression in embryonic gonads by such approaches with the small amounts of tissue available. We therefore adopted mRAP, a cloning- and sequencing-based method with a high sensitivity, for miRNA profiling in embryonic gonads.

We obtained a total of 380 miRNA-derived sequences, consisting of 374 reads for known miRNAs and six reads for previously unreported ones (four corresponding to miR-143*, one to miR-715*, and one to miR-689*). Although 2000 mRAP clones were sequenced in the present study, most of the miRNAs (both known and novel) in our data set were detected five or fewer times (Table 1), indicating that all miRNAs in the gonads may not yet have been identified. Extensive sequencing of mRAP clones may therefore result in the identification of additional novel hairpin structures containing unreported miRNA candidates.

We found that miR-29b is the most abundant miRNA in mouse gonads at E13.5. Northern blot analysis of PGC-depleted gonadal tissue further indicated that miR-29b is expressed almost exclusively in PGCs of female gonads (at least at E13.5). This finding contrasts with results of Hayashi et al. (2008) showing that miR-29b was virtually undetectable in mouse PGCs at this stage by RT-PCR analysis. This discrepancy may be attributable to the differences in methodology or in genetic background of the mice between the two studies.

Although the differences in mRAP cloning frequency between male and female gonads for some miRNAs were reflected in differences in expression as determined by Northern blot analysis, those for others were not. We have recently performed deep sequencing of mRAP clones from various mouse organs and found that the correlation between cloning frequency and Northern blot data was dependent on miRNA sequence (S Takada and H Mano, unpubl.). Even some miRNAs with a read number of >100,000 per organ were not detected by Northern blot analysis. The nucleotide sequence of miRNAs may thus greatly affect their sensitivity to detection by Northern blot analysis or by RT-PCR (a hybridization-based detection system). However, it remains possible that mRAP may have a cloning bias for some miRNAs.

Both *Dnmt3a* and *Dnmt3b* are expressed in mouse PGCs of both sexes at E13.5 (Lees-Murdock et al. 2005), suggesting

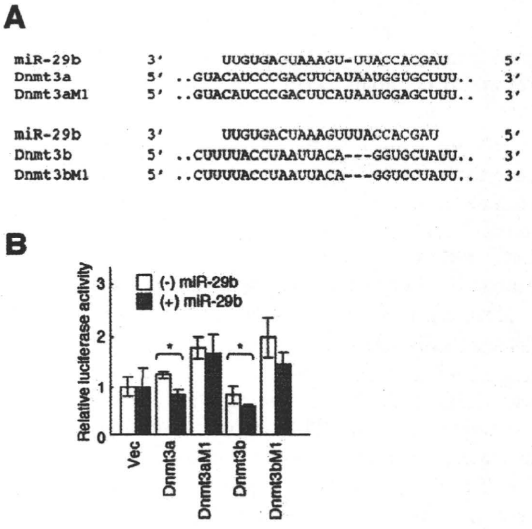

FIGURE 5. Identification of *Dnmt3a* and *Dnmt3b* as potential targets of miR-29b in mouse. (*A*) Potential target sites for miR-29b in the 3′UTRs of *Dnmt3a* and *Dnmt3b* mRNAs are shown aligned with the miR-29b sequence. The same 3′UTR sequences with a 1-bp mismatch (M1) were used as negative controls in luciferase reporter assays. Complementary bases between miR-29b (red) and the 3′UTRs (blue) are shown, respectively. (*B*) Luciferase reporter assays were performed with vectors containing DNA fragments corresponding to the putative wild-type or mutant target sites for miR-29b in the 3′UTRs of *Dnmt3a* or *Dnmt3b* mRNAs. The assays were performed in NIH3T3 cells cotransfected (or not) with the miR-29b precursor. Vec indicates cells transfected with the luciferase vector without *Dnmt3* sequences. Firefly luciferase activity was normalized by that of *Renilla* luciferase, and the data are means ± SD from three independent experiments. (*) $P < 0.05$ for the indicated comparisons (Student's *t*-test).

a possibility that DNA methylation of the genome is regulated by miR-29b. Methylation of cytosine residues is the only known direct epigenetic modification of mammalian genomic DNA and contributes to various biological phenomena including transposon silencing and genomic imprinting (Reik et al. 2001; Bird 2002). There are two main types of DNA methyltransferase: maintenance methyltransferases that methylate hemimethylated CpG sequences after DNA replication, and de novo methyltransferases that methylate cytosine residues of unmethylated CpG sequences, and which include DNMT3A and DNMT3B (Okano et al. 1998). Genome-wide demethylation occurs early during development and is complete around E13 to E14 in PGCs of both male and female mouse embryos (Monk et al. 1987; Kafri et al. 1992; Brandeis et al. 1993; Surani 1998; Tada et al. 1998). Re-methylation then takes place earlier in the male germ cells (from E15 to E16) (Kafri et al. 1992; Brandeis et al. 1993; Coffigny et al. 1999) than in the female cells (after birth, during the growth of oocytes) (Lucifero et al. 2002, 2004; Hiura et al. 2006). DNMT3A and DNMT3B were recently shown to mediate de novo methylation of differentially methylated genomic regions corresponding to imprinted genes and some repetitive elements in male germ cells (Kato et al. 2007). It is thus possible that the expression of these two enzymes is repressed by miR-29b in female germ cells, allowing an escape from male-type methylation of the genome and underlying female-type methylation.

MicroRNAs have been shown to contribute to the fine-tuning of physiological events or to function as molecular switches in cellular signaling (Lee et al. 1993; Wightman et al. 1993; Moss et al. 1997; Reinhart et al. 2000; Brennecke et al. 2003; Johnston and Hobert 2003; Sokol and Ambros 2005). In addition, some miRNAs function in a fail-safe mechanism to silence mRNAs that are unwanted in specific cell types (Hornstein et al. 2005; Cohen et al. 2006). It seems likely that miR-29b may function in such a mechanism to regulate methylation of the genome, given that the amount of *Dnmt3a* mRNA in PGCs is similar in male and female mouse embryos at E13.5 but is greater in male than in female PGCs at E15.5 and E17.5 (Iwahashi et al. 2007).

Further extensive sequencing of mRAP clones from the gonads will provide additional insight into the cell type-dependent and developmental stage-dependent expression profiles of miRNAs, and such information will likely contribute to understanding of the function of miRNAs in sex determination and differentiation.

MATERIALS AND METHODS

Mice and tissues

C57BL/6J mice (*Mus musculus domesticus*) were obtained from a local supplier (Japan SLC). The mice were allowed to mate naturally, and at noon of the day in which a vaginal plug was observed were considered to be E0.5. Gonads depleted of germ cells were prepared by intraperitoneal injection of pregnant females at E9.5 with 100 μL of a warmed solution (16 mg/mL) of busulfan (Sigma-Aldrich) in 50% dimethly sulfoxide (DMSO), and harvesting of the embryos occurred on E13.5 (Forsberg and Olivecrona 1966); as a control, dams were injected with 50% DMSO alone. The sex of each embryo was determined on the basis of the presence (male) or absence (female) of a testis cord.

Chickens and tissues

Fertilized chicken (*Gallus gallus domestica*) eggs were obtained from a local supplier (Saitama Experimental Animal Supply) and were maintained at 18°C until their transfer to an incubator at 37.8°C. Staging of chicken embryos was confirmed at dissection as described by Hamburger and Hamilton (1951). The gonads of each embryo were snap frozen, and the sex of the embryos was determined as described previously (Clinton et al. 2001; Takada et al. 2006b,c) with the use of a polymerase chain reaction (PCR)-based method performed with genomic DNA extracted from the hind limbs.

mRAP

The mRAP procedure was performed as described previously (Takada et al. 2006a; Mano and Takada 2007; Takada and Mano 2007), and miRNAs were identified from mRAP clones with the use of the computational pipeline developed by Berezikov et al. (2006b).

Northern blot analysis

A fraction of small RNA molecules (<200 nt) was prepared with the use of a mirVana miRNA Isolation Kit (Applied Biosystems), and portions of the fraction (0.5–0.8 μg per lane) were subjected to electrophoresis on a 15% polyacrylamide gel under denaturing conditions. The separated RNA molecules were transferred electrophoretically to a Hybond-N membrane (GE Healthcare UK) and were subjected to hybridization with the use of the ULTRAhyb-Oligo reagent (Applied Biosystems) and with ^{32}P-labeled locked nucleic acid (LNA) probes corresponding to reverse complementary sequences of mature miRNAs. Signals were detected with a BAS-1500 image analyzer (Fuji Photo Film), and signal intensities were measured with the use of Image Gauge version 4.1 software (Fuji Photo Film). The signal intensities of the miRNAs were normalized to that of U6 RNA. Probes included:

mmu-miR-29bRCLNA (5′-AAcACtGAtTTcAAaTGgTGcTA-3′) for miR-29b;
mmu-miR-142-3pRCLNA (5′-CCaTAaAGtAGgAAaCAcTAcA-3′) for miR-142-3p;
mmu-miR-143RCLNA (5′-TGaGCtACaGTgCTtCAtCTcA-3′) for miR-143;
mmu-miR-24RCLNA (5′-CTgTTcCTgCTgAAcTGaGCcA-3′) for miR-24;
mmu-miR-126-5pRCLNA (5′-CgCGtACcAAAAGtAAtAAtG-3′) for miR-126-5p; and
U6AS (5′-AACGCTTCACGAATTTGCGT-3′) for U6 RNA.

Here, upper- and lowercase letters designate DNA and LNA, respectively.

Whole-mount in situ hybridization

Whole-mount in situ hybridization was performed by the maleic acid buffer (MABT) method as previously described (Xu and Wilkinson 1998). A probe for *Oct4* mRNA was prepared from total RNA isolated from E12.5 mouse embryos. The RNA was subjected to reverse transcription (RT), and the resulting cDNA was subjected to PCR with the primers mOct4probe1F (5′-GCC TTGCAGCTCAGCCTTAAGA-3′) and mOct4probe1R (5′-CCTC GCCCTCAGGAAAAGGGAC-3′). The amplification product, which corresponds to the probe described by Thomas et al. (1998), was cloned into the pGEM-T Easy vector (Promega) for production of the probe by in vitro transcription.

Luciferase assay

DNA fragments corresponding to a 981-bp portion of the 3′UTR of *Dnmt3a* or a 637-bp portion of the 3′UTR of *Dnmt3b* were amplified by PCR from C57BL/6J mouse genomic DNA. The primers wereDnmt3aAmpF (5′-ACTAGTGACTGAAACAAGAGA GTTA-3′) and Dnmt3aAmpR (5′-ACGCGTGGACCGGAGCTGC CATGTGC-3′) for *Dnmt3a* and Dnmt3bAmpF (5′-ACTAGTGG TACAAGGGCTGAAGTCC-3′) and Dnmt3bAmpR (5′-ACGCGT AAGGCAGTCTCTCCCCACAC-3′) for *Dnmt3b*, with the underlined sequences corresponding to recognition sites for restriction endonucleases. The PCR products were cloned into pGEM-T Easy and verified by nucleotide sequencing. Single nucleotide substitutions were introduced into the DNA sequences with the use of a QuikChange Multi Site-Directed Mutagenesis Kit (Stratagene) and the primers Dnmt3aM1 (5′-GACTTCATAATGGAGCTTT CAAAACAG-3′) for *Dnmt3a* and Dnmt3bM1 (5′-ACCTAATTA CAGGTCCTATTTTATAG-3′) for *Dnmt3b*, with the underlined residues corresponding to the substituted bases. The insert of each clone was subcloned into the SpeI and MluI sites of the multiple cloning region of the pMIR-Report-luciferase vector (Applied Biosystems). The coding sequence and 3′UTR of the firefly luciferase cDNA as well as the insert of each of the resulting vectors were then subcloned into the BamHI and NotI sites of the pMXS vector (kindly provided by T. Kitamura, Institute of Medical Science, University of Tokyo).

NIH3T3 cells grown in 24-well plates were transfected with 50 μM miR-29b precursor (Pre-miR miRNA Precursor Molecule; Applied Biosystems), 0.6 μg of pMXS-based luciferase reporter vector, and 0.2 μg of a control *Renilla* luciferase vector (pRL-TK; Promega) in the presence of the Lipofectamine 2000 reagent (Invitrogen). Firefly and *Renilla* luciferase activities in cell lysates were assayed with the use of a Dual-Luciferase Reporter Assay System (Promega) 48 h after cell transfection, and the former activity was normalized by the latter.

ACKNOWLEDGMENTS

We thank the laboratory members for their discussions, as well as M. Otani, K. Nakamura, and S. Aoyagi for technical assistance. This work was supported in part by Grants-in-Aid for Scientific Research from the Ministry of Education, Culture, Sports, Science and Technology of Japan (to S.T.); a grant for Third-Term Comprehensive Control Research for Cancer from the Ministry of Health, Labor, and Welfare of Japan (to H.M.); and a grant for Scientific Research on Priority Areas "Applied Genomics" from the Ministry of Education, Culture, Sports, Science and Technology of Japan (to H.M.).

Received October 14, 2008; accepted April 27, 2009.

REFERENCES

Aboobaker AA, Tomancak P, Patel N, Rubin GM, Lai EC. 2005. *Drosophila* microRNAs exhibit diverse spatial expression patterns during embryonic development. *Proc Natl Acad Sci* **102:** 18017–18022.

Andl T, Murchison EP, Liu F, Zhang Y, Yunta-Gonzalez M, Tobias JW, Andl CD, Seykora JT, Hannon GJ, Millar SE. 2006. The miRNA-processing enzyme dicer is essential for the morphogenesis and maintenance of hair follicles. *Curr Biol* **16:** 1041–1049.

Ason B, Darnell DK, Wittbrodt B, Berezikov E, Kloosterman WP, Wittbrodt J, Antin PB, Plasterk RH. 2006. Differences in vertebrate microRNA expression. *Proc Natl Acad Sci* **103:** 14385–14389.

Bartel DP. 2004. MicroRNAs: Genomics, biogenesis, mechanism, and function. *Cell* **116:** 281–297.

Berezikov E, Thuemmler F, van Laake LW, Kondova I, Bontrop R, Cuppen E, Plasterk RH. 2006a. Diversity of microRNAs in human and chimpanzee brain. *Nat Genet* **38:** 1375–1377.

Berezikov E, van Tetering G, Verheul M, van de Belt J, van Laake L, Vos J, Verloop R, van de Wetering M, Guryev V, Takada S, et al. 2006b. Many novel mammalian microRNA candidates identified by extensive cloning and RAKE analysis. *Genome Res* **16:** 1289–1298.

Bernstein E, Kim SY, Carmell MA, Murchison EP, Alcorn H, Li MZ, Mills AA, Elledge SJ, Anderson KV, Hannon GJ. 2003. Dicer is essential for mouse development. *Nat Genet* **35:** 215–217.

Bird A. 2002. DNA methylation patterns and epigenetic memory. *Genes & Dev* **16:** 6–21.

Brandeis M, Kafri T, Ariel M, Chaillet JR, McCarrey J, Razin A, Cedar H. 1993. The ontogeny of allele-specific methylation associated with imprinted genes in the mouse. *EMBO J* **12:** 3669–3677.

Brennecke J, Hipfner DR, Stark A, Russell RB, Cohen SM. 2003. *bantam* encodes a developmentally regulated microRNA that controls cell proliferation and regulates the proapoptotic gene *hid* in *Drosophila*. *Cell* **113:** 25–36.

Carre-Eusebe D, di Clemente N, Rey R, Pieau C, Vigier B, Josso N, Picard JY. 1996. Cloning and expression of the chick anti-Müllerian hormone gene. *J Biol Chem* **271:** 4798–4804.

Carrington JC, Ambros V. 2003. Role of microRNAs in plant and animal development. *Science* **301:** 336–338.

Clinton M, Haines L, Belloir B, McBride D. 2001. Sexing chick embryos: A rapid and simple protocol. *Br Poult Sci* **42:** 134–138.

Coffigny H, Bourgeois C, Ricoul M, Bernardino J, Vilain A, Niveleau A, Malfoy B, Dutrillaux B. 1999. Alterations of DNA methylation patterns in germ cells and Sertoli cells from developing mouse testis. *Cytogenet Cell Genet* **87:** 175–181.

Cohen SM, Brennecke J, Stark A. 2006. Denoising feedback loops by thresholding—A new role for microRNAs. *Genes & Dev* **20:** 2769–2772.

Fabbri M, Garzon R, Cimmino A, Liu Z, Zanesi N, Callegari E, Liu S, Alder H, Costinean S, Fernandez-Cymering C, et al. 2007. MicroRNA-29 family reverts aberrant methylation in lung cancer by targeting DNA methyltransferases 3A and 3B. *Proc Natl Acad Sci* **104:** 15805–15810.

Filipowicz W. 2005. RNAi: The nuts and bolts of the RISC machine. *Cell* **122:** 17–20.

Forsberg JG, Olivecrona H. 1966. The effect of prenatally administered Busulphan on rat gonads. *Biol Neonat* **10:** 180–192.

Grimson A, Farh KK, Johnston WK, Garrett-Engele P, Lim LP, Bartel DP. 2007. MicroRNA targeting specificity in mammals: Determinants beyond seed pairing. *Mol Cell* **27:** 91–105.

Gubbay J, Collignon J, Koopman P, Capel B, Economou A, Münsterberg A, Vivian N, Goodfellow P, Lovell-Badge R. 1990.

A gene mapping to the sex-determining region of the mouse Y chromosome is a member of a novel family of embryonically expressed genes. *Nature* **346:** 245–250.

Hamburger V, Hamilton HL. 1951. A series of normal stages in the development of the chick embryo. *J Morphol* **88:** 49–92.

Hammond SM. 2005. Dicing and slicing: The core machinery of the RNA interference pathway. *FEBS Lett* **579:** 5822–5829.

Hannon GJ. 2002. RNA interference. *Nature* **418:** 244–251.

Harfe BD, McManus MT, Mansfield JH, Hornstein E, Tabin CJ. 2005. The RNaseIII enzyme Dicer is required for morphogenesis but not patterning of the vertebrate limb. *Proc Natl Acad Sci* **102:** 10898–10903.

Harris KS, Zhang Z, McManus MT, Harfe BD, Sun X. 2006. Dicer function is essential for lung epithelium morphogenesis. *Proc Natl Acad Sci* **103:** 2208–2213.

Hayashi K, Chuva de Sousa Lopes SM, Kaneda M, Tang F, Hajkova P, Lao K, O'Carroll D, Das PP, Tarakhovsky A, Miska EA, et al. 2008. MicroRNA biogenesis is required for mouse primordial germ cell development and spermatogenesis. *PLoS One* **3:** e1738. doi: 10.1371/journal.pone.0001738.

Hiura H, Obata Y, Komiyama J, Shirai M, Kono T. 2006. Oocyte growth-dependent progression of maternal imprinting in mice. *Genes Cells* **11:** 353–361.

Hornstein E, Mansfield JH, Yekta S, Hu JK, Harfe BD, McManus MT, Baskerville S, Bartel DP, Tabin CJ. 2005. The microRNA miR-196 acts upstream of Hoxb8 and Shh in limb development. *Nature* **438:** 671–674.

Iwahashi K, Yoshioka H, Low EW, McCarrey JR, Yanagimachi R, Yamazaki Y. 2007. Autonomous regulation of sex-specific developmental programming in mouse fetal germ cells. *Biol Reprod* **77:** 697–706.

Johnston RJ, Hobert O. 2003. A microRNA controlling left/right neuronal asymmetry in *Caenorhabditis elegans*. *Nature* **426:** 845–849.

Kafri T, Ariel M, Brandeis M, Shemer R, Urven L, McCarrey J, Cedar H, Razin A. 1992. Developmental pattern of gene-specific DNA methylation in the mouse embryo and germ line. *Genes & Dev* **6:** 705–714.

Kato Y, Kaneda M, Hata K, Kumaki K, Hisano M, Kohara Y, Okano M, Li E, Nozaki M, Sasaki H. 2007. Role of the Dnmt3 family in de novo methylation of imprinted and repetitive sequences during male germ cell development in the mouse. *Hum Mol Genet* **16:** 2272–2280.

Kent J, Wheatley SC, Andrews JE, Sinclair AH, Koopman P. 1996. A male-specific role for SOX9 in vertebrate sex determination. *Development* **122:** 2813–2822.

Kloosterman WP, Plasterk RH. 2006. The diverse functions of microRNAs in animal development and disease. *Dev Cell* **11:** 441–450.

Kloosterman WP, Wienholds E, de Bruijn E, Kauppinen S, Plasterk RH. 2006. In situ detection of miRNAs in animal embryos using LNA-modified oligonucleotide probes. *Nat Methods* **3:** 27–29.

Koopman P, Gubbay J, Vivian N, Goodfellow P, Lovell-Badge R. 1991. Male development of chromosomally female mice transgenic for Sry. *Nature* **351:** 117–121.

Lagos-Quintana M, Rauhut R, Yalcin A, Meyer J, Lendeckel W, Tuschl T. 2002. Identification of tissue-specific microRNAs from mouse. *Curr Biol* **12:** 735–737.

Lee RC, Feinbaum RL, Ambros V. 1993. The *C. elegans* heterochronic gene *lin-4* encodes small RNAs with antisense complementarity to *lin-14*. *Cell* **75:** 843–854.

Lees-Murdock DJ, Shovlin TC, Gardiner T, De Felici M, Walsh CP. 2005. DNA methyltransferase expression in the mouse germ line during periods of de novo methylation. *Dev Dyn* **232:** 992–1002.

Lewis BP, Shih IH, Jones-Rhoades MW, Bartel DP, Burge CB. 2003. Prediction of mammalian microRNA targets. *Cell* **115:** 787–798.

Loffler KA, Zarkower D, Koopman P. 2003. Etiology of ovarian failure in blepharophimosis ptosis epicanthus inversus syndrome: FOXL2 is a conserved, early-acting gene in vertebrate ovarian development. *Endocrinology* **144:** 3237–3243.

Lucifero D, Mertineit C, Clarke HJ, Bestor TH, Trasler JM. 2002. Methylation dynamics of imprinted genes in mouse germ cells. *Genomics* **79:** 530–538.

Lucifero D, Mann MR, Bartolomei MS, Trasler JM. 2004. Gene-specific timing and epigenetic memory in oocyte imprinting. *Hum Mol Genet* **13:** 839–849.

Mano H, Takada S. 2007. mRAP, a sensitive method for determination of microRNA expression profiles. *Methods* **43:** 118–122.

Mattick JS, Makunin IV. 2005. Small regulatory RNAs in mammals. *Hum Mol Genet* **14:** R121–R132.

Monk M, Boubelik M, Lehnert S. 1987. Temporal and regional changes in DNA methylation in the embryonic, extraembryonic and germ cell lineages during mouse embryo development. *Development* **99:** 371–382.

Morais da Silva S, Hacker A, Harley V, Goodfellow P, Swain A, Lovell-Badge R. 1996. Sox9 expression during gonadal development implies a conserved role for the gene in testis differentiation in mammals and birds. *Nat Genet* **14:** 62–68.

Moss EG, Lee RC, Ambros V. 1997. The cold shock domain protein LIN-28 controls developmental timing in *C. elegans* and is regulated by the *lin-4* RNA. *Cell* **88:** 637–646.

Okano M, Xie S, Li E. 1998. Cloning and characterization of a family of novel mammalian DNA (cytosine-5) methyltransferases. *Nat Genet* **19:** 219–220.

Pesce M, Wang X, Wolgemuth DJ, Schöler H. 1998. Differential expression of the Oct-4 transcription factor during mouse germ cell differentiation. *Mech Dev* **71:** 89–98.

Reik W, Dean W, Walter J. 2001. Epigenetic reprogramming in mammalian development. *Science* **293:** 1089–1093.

Reinhart BJ, Slack FJ, Basson M, Pasquinelli AE, Bettinger JC, Rougvie AE, Horvitz HR, Ruvkun G. 2000. The 21-nucleotide *let-7* RNA regulates developmental timing in *Caenorhabditis elegans*. *Nature* **403:** 901–906.

Sokol NS, Ambros V. 2005. Mesodermally expressed *Drosophila* microRNA-1 is regulated by Twist and is required in muscles during larval growth. *Genes & Dev* **19:** 2343–2354.

Surani MA. 1998. Imprinting and the initiation of gene silencing in the germ line. *Cell* **93:** 309–312.

Tada T, Tada M, Hilton K, Barton SC, Sado T, Takagi N, Surani MA. 1998. Epigenotype switching of imprintable loci in embryonic germ cells. *Dev Genes Evol* **207:** 551–561.

Takada S, Mano H. 2007. Profiling of microRNA expression by mRAP. *Nat Protocols* **2:** 3136–3145.

Takada S, Berezikov E, Yamashita Y, Lagos-Quintana M, Kloosterman WP, Enomoto M, Hatanaka H, Fujiwara S, Watanabe H, Soda M, et al. 2006a. Mouse microRNA profiles determined with a new and sensitive cloning method. *Nucleic Acids Res* **34:** e115. doi: 10.1093/nar/gkl653.

Takada S, Ota J, Kansaku N, Yamashita H, Izumi T, Ishikawa M, Wada T, Kaneda R, Choi YL, Koinuma K, et al. 2006b. Nucleotide sequence and embryonic expression of quail and duck Sox9 genes. *Gen Comp Endocrinol* **145:** 208–213.

Takada S, Wada T, Kaneda R, Choi YL, Yamashita Y, Mano H. 2006c. Evidence for activation of Amh gene expression by steroidogenic factor 1. *Mech Dev* **123:** 472–480.

Thomas PQ, Brown A, Beddington RS. 1998. Hex: A homeobox gene revealing peri-implantation asymmetry in the mouse embryo and an early transient marker of endothelial cell precursors. *Development* **125:** 85–94.

Wienholds E, Kloosterman WP, Miska E, Alvarez-Saavedra E, Berezikov E, de Bruijn E, Horvitz HR, Kauppinen S, Plasterk RH. 2005. MicroRNA expression in zebrafish embryonic development. *Science* **309:** 310–311.

Wightman B, Ha I, Ruvkun G. 1993. Posttranscriptional regulation of the heterochronic gene *lin-14* by *lin-4* mediates temporal pattern formation in *C. elegans*. *Cell* **75:** 855–862.

Xu Q, Wilkinson D. 1998. In situ hybridization of mRNA with hapten labelled probes. In *In situ hybridization: A practical approach*, 2nd ed. (ed. D Wilkinson), pp. 87–106. Oxford University Press, Oxford, UK.

Yi R, O'Carroll D, Pasolli HA, Zhang Z, Dietrich FS, Tarakhovsky A, Fuchs E. 2006. Morphogenesis in skin is governed by discrete sets of differentially expressed microRNAs. *Nat Genet* **38:** 356–362.

Screening for genetic abnormalities involved in ovarian carcinogenesis using retroviral expression libraries

TOMOAKI WADA[1,2], YOSHIHIRO YAMASHITA[1], YASUSHI SAGA[2], KAYOKO TAKAHASHI[2], KOJI KOINUMA[1], YOUNG LIM CHOI[1], RURI KANEDA[1], SHIN-ICHIRO FUJIWARA[1], MANABU SODA[1], HIDEKI WATANABE[1], KENTARO KURASHINA[1], HISASHI HATANAKA[1], MUNEHIRO ENOMOTO[1], SHUJI TAKADA[1], HIROYUKI MANO[1,3] and MITSUAKI SUZUKI[2]

[1]Division of Functional Genomics and [2]Department of Obstetrics and Gynecology, School of Medicine, Jichi Medical University, Tochigi; [3]CREST, Japan Science and Technology Agency, Saitama, Japan

Received April 24, 2009; Accepted June 23, 2009

DOI: 10.3892/ijo_00000410

Abstract. The purpose of this study was to screen for genes involved in ovarian carcinogenesis in an attempt to develop an effective molecular-targeted therapy for ovarian cancer. We constructed retroviral expression libraries for the human ovarian cancer cell lines SHIN-3 and TYK-CPr, and performed a focus formation assay with 3T3 cells. As a result, *proteasome subunit beta-type 2 (PSMB2), ubiquitin-specific protease 14 (USP14)*, and *keratin 8 (KRT8)* were identified from SHIN-3, and *polymerase II RNA subunit (POLR2E), chaperonin containing T-complex polypeptide 1 subunit 4 (CCT4), glia maturation factor beta (GMFB)*, and *neuroblastoma ras viral oncogene homolog (NRAS)* from TYK-CPr. *NRAS* gene analysis revealed a CAA→AAA substitution at codon 61, resulting in a Glu→Lys change at position 61. When the mutant *NRAS* was introduced into fibroblasts for its expression, many transformed foci were generated, confirming the transforming ability of the mutant *NRAS*.

Introduction

Ovarian cancer is the fifth most common cause of death from gynecologic malignancies in the USA. Approximately 25,000 women are affected by ovarian cancer every year, and about 14,000 die of this disease (1). In recent years, debulking surgery followed by multidrug therapy with platinum and taxine drugs have been used, with some improvement in prognosis (2); however, the 5-year survival rate remains at about 50% (3). This is due to the lack of effective therapy for treatment-resistant or recurrent ovarian cancer.

A series of recent studies have reported that STI571, which targets the *BCR-ABL* gene responsible for chronic myelogenous leukemia, is effective for this disease, and that the anti-CD20 antibody rituximab is highly effective for B-cell lymphocytic leukemia (4). These observations have demonstrated that it is clinically very important to elucidate the pathogenesis of malignancies and thereby develop molecular-targeted therapy for them. To improve the prognosis of patients with ovarian cancer, it is important to define genetic abnormalities involved in the onset of this disease, and to develop effective molecular-targeted therapies for ovarian cancer.

To date, several studies have reported that mutations in the *p53* gene (5) or deletions in the *BRCA1* and *BRCA2* genes (6) are common in ovarian cancer. However, there is no evidence that these genetic abnormalities are directly involved in the development of ovarian cancer.

In a recent study, we constructed a full-length cDNA expression library of non-small cell lung cancer (NSCLC) using a retroviral vector, and demonstrated by functional screening that a fusion gene, composed of portions of the echinoderm microtubule-associated protein-like 4 (*EML4*) and anaplastic lymphoma kinase (*ALK*) genes, was involved in the development of NSCLC (7). In this study, we aimed to screen for genes responsible for ovarian carcinogenesis using similar techniques.

Materials and methods

Cell culture. Ovarian serous cystadenocarcinoma cell line SHIN-3 (8) and ovarian undifferentiated carcinoma cell line TYK-CPr (JCRB0234.1, Health Science Research Resources Bank: HSRRB, Osaka, Japan) (9) cells were cultured in Dulbecco's modified Eagle's medium/F12 (DMEM/F12; Invitrogen, Carlsbad, CA, USA) medium supplemented with 10% fetal bovine serum (Invitrogen), 2 mM L-glutamine (Invitrogen), and 1% penicillin-streptomycin (Invitrogen). The BOSC23 packaging cell line for ecotropic retroviruses (10) and mouse 3T3 fibroblasts (American Type Culture

Correspondence to: Dr Yasushi Saga, Department of Obstetrics and Gynecology, School of Medicine, Jichi Medical university, 3311-1 Yakushiji, Shimotsuke, Tochigi 329-0498, Japan
E-mail: saga@jichi.ac.jp

Key words: ovarian cancer, oncogene, retroviral expression screening, NRAS

Collection: ATCC) were maintained in DMEM/F12 supplemented with 10% fetal bovine serum and 2 mM L-glutamine, and 1% penicillin-streptomycin.

Construction of a retrovirus library. Total RNA was extracted from SHIN-3 and TYK-CPr cells with the use of an RNeasy Mini column and RNase-free DNase (Qiagen, Valencia, CA, USA), and first-strand cDNA was synthesized from the RNA with PowerScript reverse transcriptase, a SMART IIA oligonucleotide, and CDS primer IIA (Clontech, Palo Alto, CA, USA). The resulting cDNA molecules were then amplified for 15 cycles with the 5'-PCR primer IIA and a SMART PCR cDNA synthesis kit (Clontech), with the exception that LA Taq polymerase (Takara Bio, Shiga, Japan) was substituted for the Advantage 2 DNA polymerase provided with the kit. The PCR products were treated with proteinase K, rendered blunt-ended with T4 DNA polymerase, and ligated to a *BstXI* adapter (Invitrogen). Unbound adapters were removed with a cDNA size fractionation column (Invitrogen), and the modified cDNAs were ligated into the pMX retroviral plasmid (11) that had been digested with *BstXI*. The pMX-cDNA plasmids were introduced into ElecroMax DH10B cells (Invitrogen) by electroporation.

Focus formation assay. BOSC23 cells ($1.8x10^6$) were seeded onto 6-cm culture plates, cultured for 1 day, and then transfected with a mixture comprising 2 μg of retroviral plasmids, 0.5 μg of pGP plasmid (Takara Bio), 0.5 μg of pE-eco plasmid (Takara Bio), and 18 μl of Lipofectamine reagent (Invitrogen). Two days after transfection, polybrene (Sigma, St. Louis, MO, USA) was added at a concentration of 4 μg/ml to the culture supernatant, which was then used to infect 3T3 cells for 48 h. For the focus formation assay, the culture medium of 3T3 cells was changed to DMEM-high glucose (Invitrogen) supplemented with 5% calf serum and 2 mM L-glutamine. Transformed foci were isolated after 3 weeks of culture.

Recovery of cDNAs from 3T3 cells. Each 3T3 cell clone was harvested with a cloning syringe and cultured independently in a 10-cm culture plate. Genomic DNA was subsequently extracted from the cells and subjected to PCR with the 5'-PCR primer IIA and LA Taq polymerase for 50 cycles of 98˚C for 20 sec and 68˚C for 6 min. Amplified genomic fragments were purified by gel electrophoresis and ligated into the pT7Blue-2 vector (EMD Biosciences, San Diego, CA, USA) for nucleotide sequencing. The cDNAs obtained were introduced into the pMXS plasmid to prepare a recombinant retrovirus, which was used again to test its 3T3-transforming ability.

Analysis of the NRAS gene in the TYK-CPr cell line. Using as the substrate the cDNA that had been synthesized to construct the retroviral library, along with NRAS primers [5' primer (GTGGAGCTTGAGGTTCTTGC) and 3' primer (GCAG CTTGAAAGTGGCTCTT)], the *NRAS* gene was amplified by PCR for 30 cycles of 98˚C for 30 sec, 62˚C for 30 sec, and 68˚C for 30 sec. The amplified DNA fragments were separated by electrophoresis, then purified, and inserted into the pGEM-T Easy Vector (Promega Corp., Madison, WI, USA) for sequencing.

Results

Construction of full-length cDNA expression libraries for SHIN-3 and TYK-CPr cells. cDNAs from SHIN-3 and TYK-CPr cells were inserted into the pMXS retroviral plasmid, which was then introduced into DH10B cells by electroporation. As a result, we obtained plasmid libraries of cDNA clones from SHIN-3 ($1.1x10^6$ colony-forming units, or cfu) and TYK-CPr ($1.2x10^6$ cfu) cells. From each of these plasmid clone libraries, 24 clones were picked up at random. In addition, to ascertain whether the cDNA inserts were full-length (complete reading frame), 10 clones were selected from each library, and ~500 bp of both ends of the cDNA insert were sequenced. The identified sequences were compared with the University of California-Santa Cruz Genome Browser Database (http://genome.ucsc.edu) by BLAST search (12). As a result, 7 of the 10 TYK-CPr-derived clones and 7 of the 10 SHIN-3-derived clones contained full-length cDNA inserts (data not shown). We therefore concluded that the retroviral cDNA expression libraries were of sufficient complexity and adequately enriched in full-length cDNAs for the present study.

Screening for transformed clones. 3T3 cells were transfected with retroviral cDNA expression libraries, and, after 3 weeks of culture, transformed clones were isolated. As a result, 17 and 15 transformed clones were identified for TYK-CPr and SHIN-3, respectively (Fig. 1).

Transformed clones were isolated using a cloning syringe, and cultured in separate dishes to extract genomic DNA from each clone. The genomic DNA was amplified by PCR using the same primers as those employed in cDNA amplification for library construction. As shown in Fig. 2, a single sharp cDNA band per clone was identified in about half of the clones.

Analysis of cDNAs recovered from transformed cells. Transformed clones, whose genomic DNA amplified by PCR gave a single sharp cDNA band, were selected, and their respective cDNAs were sequenced for gene identification. As a result, *proteasome subunit beta-type 2 (PSMB2), ubiquitin-specific protease 14 (USP14)*, and *keratin 8 (KRT8)* were identified from SHIN-3, and *polymerase II RNA subunit (POLR2E), chaperonin containing T-complex polypeptide 1 subunit 4 (CCT4), glia maturation factor beta (GMFB)*, and *neuroblastoma ras viral oncogene homolog (NRAS)* from TYK-CPr. All cDNAs contained complete open reading frames (ORF).

Analysis of the NRAS gene in the TYK-CPr cell line. Focusing on *NRAS* among the genes identified in this study, we examined the TYK-CPr-derived cDNA for point mutations, and found a codon 61 mutation (CAA→AAA, Glu→Lys) (Fig. 3).

Furthermore, the resulting mutant NRAS ($NRAS^{Q61K}$) cDNA was inserted into the pMX plasmid to construct a recombinant retrovirus, which was transfected into 3T3 cells for a focus formation assay. As shown in Fig. 4, the identified $NRAS^{Q61K}$ generated many transformed foci, confirming its transforming ability.

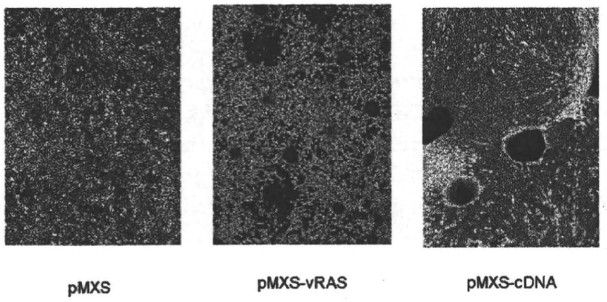

Figure 1. Focus formation assay with a retroviral library derived from TYK-CPr cells. Mouse 3T3 cells were infected with the empty virus (pMXS), a retrovirus expressing v-Ras as a positive control (pMXS-vRAS), or retroviruses from the TYK-CPr cell library (pMXS-cDNA). The cultures were photographed 3 weeks after infection.

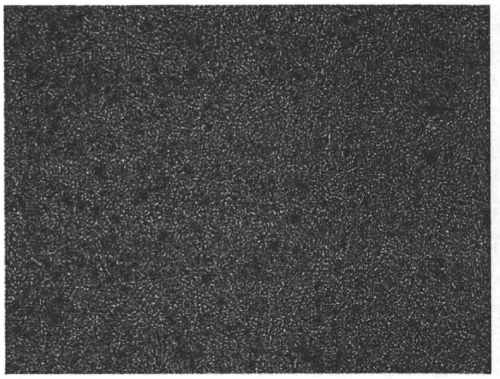

Figure 4. A recombinant retrovirus encoding $NRAS^{Q61K}$ was used to infect 3T3 cells. The cells were photographed after culture for 2 weeks.

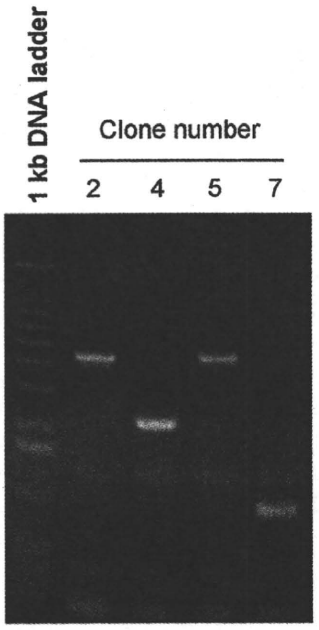

Figure 2. Genomic DNA isolated from transformed 3T3 cell foci (clone numbers 2, 4, 5, and 7) was subjected to PCR for amplification of the DNA inserts. The left lane contains DNA size markers (1-kbp DNA ladder; Invitrogen).

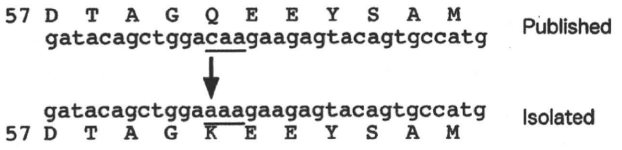

Figure 3. The amino acid sequence in the vicinity of the amino acid residue at position 61 of NRAS protein and the corresponding NRAS cDNA (NM_002524) codon sequence are shown in the upper row (published). Similarly, the amino acid sequence and the corresponding NRAS cDNA (isolated) codon sequence identified in this study are shown in the lower row. In the screened cDNA, the glutamine-encoding codon (caa) at position 61 had been converted to the lysine-encoding codon (aaa). The site of the nucleotide substitution is indicated in red.

To confirm that the $NRAS^{Q61K}$ mutation did not arise during the process of library construction or PCR, we sequenced the *NRAS* gene in 10 randomly selected TYK-CPr cell clones, and found a CAA→AAA substitution at codon 61 in 7 clones. This indicates that the TYK-CPr cell line has a wild-type allele and a mutant allele ($NRAS^{Q61K}$).

Discussion

The focus formation assay in mouse 3T3 fibroblasts has been widely used to identify oncogenes (13). The conventional 3T3 focus formation assay involves the introduction of cancer cell-derived genomic DNA, followed by screening for focus-forming, transformed clones of 3T3 cells. To date, many oncogenes such as *RAS, ABL*, and *RAF* have been identified using this assay. However, the assay involving the introduction of genomic DNA alone has the major disadvantage of a lower screening ability, that is, the expression of oncogenes is controlled by their own enhancer/promoter region. However, the enhancer/promoter region of oncogenes functioning in ovarian cancer is not necessarily active in 3T3 fibroblasts. Therefore, the possibility of the successful identification of ovarian cancer-related oncogenes by the classical focus formation assay involving the introduction of genomic DNA alone is small. To ensure that all genes introduced into 3T3 cells are expressed at sufficient levels, it is necessary that their transcription be regulated by exogenous promoters and enhancers.

The retroviral vector is a type of vector most commonly used for gene introduction, and has advantages in that the cDNA inserted between the left and right long terminal repeats (LTR) is integrated directly into the chromosomes of infected cells, and viral vectors can be produced at high titers using packaging cells (14,15).

In this study, to screen for genes involved in ovarian carcinogenesis, we attempted to construct cDNA-expressing recombinant retroviral libraries that were engineered to express cDNA from retroviral LTR, and succeeded in constructing libraries with a sufficient complexity and mean insert size, derived from the ovarian cancer cell lines SHIN-3 and TYK-CPr. Using these libraries, we performed a focus formation assay in 3T3 cells, and were able to recover the cDNA inserts easily from the transformed clones employing the primers used for cDNA synthesis. From each of 7 clones, a single cDNA was identified and sequenced. As a result, *PSMB2, USP14*, and *KRT8* were screened from SHIN-3 cells, and *POLR2E, CCT4, GMFB*, and *NRAS* from TYK-CPr

cells. Focusing on *NRAS*, known as an oncogene, we analyzed it, and identified a CAA→AAA substitution at codon 61, resulting in a Glu→Lys change at position 61. When the mutant *NRAS* was transfected into fibroblasts for its expression, many transformed foci were generated, confirming the transforming ability of the mutant *NRAS*.

The RAS gene family is a group of three oncogenes, KRAS, HRAS, and NRAS, which are most commonly activated in human malignant neoplasms (16). For RAS activation, an amino acid substitution at position 12, 13, 59, or 61 is important. It was reported in thyroid tumors that a CAA→CGA substitution at codon 61 of NRAS resulted in a Glu→Arg change at position 61 and NRAS activation (17). It was also noted in the neuroblastoma cell line SK-N-SH that a Glu→Lys mutation at position 61 of NRAS resulted in its activation (18).

Furthermore, KRAS mutations were reported to occur in about 50% of ovarian mucinous carcinomas (19,20) and 30% of serous borderline ovarian tumors (21). In addition, HRAS mutations were reported in about 6% of ovarian cancers (22). However, no NRAS activation in ovarian cancers has been reported to date (22). Since the cell proliferation function of the HRAS, KRAS, and NRAS gene products overlaps with one another in many cases, the reason for selective KRAS activation in specific histological types of ovarian cancer is unclear.

This study is the first in the world to identify *NRAS* gene activation by point mutation in an ovarian cancer cell line. However, no *NRAS* gene activation has been reported in ovarian cancer patients. In the future, it will be necessary to analyze clinical samples for NRAS mutations, particularly amino acid substitutions at position 61. TYK-CPr, in which an activated NRAS gene was identified in this study, is a cell line derived from an undifferentiated ovarian cancer with a clinically poor prognosis. This suggests that NRAS activation is associated with specific histological types of ovarian cancer.

Recently, sorafenib, a molecular-targeted therapeutic drug targeting activated RAS, has been developed and used clinically. The drug inhibits Raf kinase downstream of RAS, thereby blocking the RAS/MEK/ERK signaling pathway and exerting antitumor effects (23). Such a molecular-targeted drug may be effective for ovarian cancer patients with the NRAS mutations reported here.

Among the genes screened in this study, proteasome has been reported to be involved in cell cycle regulation and apoptosis (24). In addition, *keratin 8* has been reported to be involved in malignant transformation and cancer cell invasion (25). These genes may be ovarian cancer-related oncogenes, although further studies are needed.

References

1. Jemal A, Siegel R and Ward E: Cancer statistics, 2008. CA Cancer J Clin 58: 71-76, 2008.
2. Armstrong DK, Bundy B and Wenzel L: Intraperitoneal cisplatin and paclitaxel in ovarian cancer. N Engl J Med 354: 34-43, 2006.
3. Druker BJ, Talpaz M and Resta DJ: Efficacy and safety of a specific inhibitor of the BCR-ABL tyrosine kinase in chronic myeloid leukemia. N Engl J Med 344: 1031-1037, 2001.
4. Maloney DG, Grillo-Lopez AJ and White CA: IDEC-C2B8 (Rituximab) anti-CD20 monoclonal antibody therapy in patients with relapsed low-grade non-Hodgkin's lymphoma. Blood 90: 2188-2195, 1997.
5. Okamoto A, Sameshima Y and Yokoyama S: Frequent allelic losses and mutations of the p53 gene in human ovarian cancer. Cancer Res 51: 5171-5176, 1991.
6. Esteller M, Silva JM and Dominguez G: Promoter hypermethylation and BRCA1 inactivation in sporadic breast and ovarian tumors. J Natl Cancer Inst 92: 564-569, 2000.
7. Soda M, Choi YL and Enomoto M: Identification of the transforming EML4-ALK fusion gene in non-small-cell lung cancer. Nature 448: 545-546, 2007.
8. Imai S, Kiyozuka Y and Maeda H: Establishment and characterization of a human ovarian serous cystadenocarcinoma cell line that produces the tumor markers CA-125 and tissue polypeptide antigen. Oncology 47: 177-184, 1990.
9. Yoshizawa H, Adashi S and Misawa Y: Isolation of cisplatin-resistant subline from human ovarian cancer cell line and analysis of its cell-biological characteristics (in Japanese). Nihon Sanfujinka Gakkai-shi 141: 7-14, 1989.
10. Pear WS, Nolan GP and Scott ML: Production of high-titer helper-free retroviruses by transient transfection. Proc Natl Acad Sci USA 90: 8392-8396, 1993.
11. Onishi M, Kinoshita S and Morikawa Y: Applications of retrovirus-mediated expression cloning. Exp Hematol 24: 324-329, 1996.
12. Kent WJ: BLAT - the BLAST-like alignment tool. Genome Res 12: 656-664, 2002.
13. Aaronson SA: Growth factors and cancer. Science 254: 1146-1153, 1991.
14. Kisanuki H, Choi YL and Wada T: Retroviral expression screening of oncogenes in pancreatic ductal carcinoma. Eur J Cancer 41: 2170-2175, 2005.
15. Choi YL, Moriuchi R and Osawa M: Retroviral expression screening of oncogenes in natural killer cell leukemia. Leuk Res 29: 943-949, 2005.
16. Shih TY and Weeks MO: Oncogenes and cancer: the p21 ras genes. Cancer Invest 2: 109-123, 1984.
17. Nikiforova MN, Lynch RA and Biddinger PW: RAS point mutations and PAX8-PPAR gamma rearrangement in thyroid tumors: evidence for distinct molecular pathways in thyroid follicular carcinoma. J Clin Endocrinol Metab 88: 2318-2326, 2003.
18. Taparowsky E, Shimizu K and Goldfarb M: Structure and activation of the human N-ras gene. Cell 34: 581-586, 1983.
19. Ichikawa Y, Nishida M and Suzuki H: Suppression of metastasis of rat prostatic cancer by introducing human chromosome 8. Cancer Res 54: 2299-2302, 1994.
20. Suzuki M, Saito S and Saga Y: Mutation of K-RAS proto-oncogene and loss of heterozygosity on 6q27 in serous and mucinous ovarian carcinomas. Cancer Genet Cytogenet 118: 132-135, 2000.
21. Shih IeM and Kurman RJ: Molecular pathogenesis of ovarian borderline tumors: new insights and old challenges. Clin Cancer Res 11: 7273-7279, 2005.
22. Mammas IN, Zafiropoulos A and Spandidos DA: Involvement of the ras genes in female genital tract cancer (review). Int J Oncol 26: 1241-1255, 2005.
23. Zhang X, Vincent P and McHugh M: BAY 43-9006 exhibits broad spectrum oral antitumor activity and targets the RAF/MEK/ERK pathway and receptor tyrosine kinases involved in tumor progression and angiogenesis. Cancer Res 64: 7099-7109, 2004.
24. Wilhelm SM, Carter C and Tang L: Proteasome inhibition and its clinical prospects in the treatment of hematologic and solid malignancies. Cancer 104: 1794-1807, 2005.
25. Hendrix MJC, Seftor EA and Chu YW: Role of intermediate filaments in migration, invasion and metastasis. Cancer Metastasis Rev 15: 507-525, 1996.

Cancer Chemother Pharmacol (2009) 64:1129–1137
DOI 10.1007/s00280-009-0974-0

ORIGINAL ARTICLE

Schedule-dependent synergism and antagonism between pemetrexed and docetaxel in human lung cancer cell lines in vitro

Yasuhiko Kano · Masaru Tanaka · Miyuki Akutsu · Kiyoshi Mori · Yasuo Yazawa · Hiroyuki Mano · Yusuke Furukawa

Received: 26 August 2008 / Accepted: 27 February 2009 / Published online: 22 March 2009

Abstract
Background Pemetrexed and docetaxel show clinical activities against a variety of solid tumors including lung cancers. To identify the optimal schedule for combination, cytotoxic interactions between pemetrexed and docetaxel were studied at various schedules using three human lung cancer cell lines A-549, Lu-99, and SBC-5 in vitro.
Methods Cells were incubated with pemetrexed and docetaxel simultaneously for 24 or 120 h. Cells were also incubated with pemetrexed for 24 h, followed by a 24 h exposure to docetaxel, and vice versa. Growth inhibition was determined using 3-(4,5-dimethylthiazol-2-yl)-2,5-diphenyltetrazolium bromide (MTT) assay and cell cycle analysis. Cytotoxic interactions were evaluated by the isobologram method.
Results Simultaneous exposure to pemetrexed and docetaxel for 24 and 120 h produced antagonistic effects in all three cell lines. Pemetrexed (24 h) followed by docetaxel (24 h) produced additive effects in A-549 cells and synergistic effects in Lu-99 and SBC-5 cells. Docetaxel followed by pemetrexed produced additive effects in A-549 and Lu-99 cells and antagonistic effects in SBC-5 cells. The results of cell cycle analysis were fully consistent with those of isobologram analysis, and provide the molecular basis of the sequence-dependent difference in cytotoxic interactions between the two agents.
Conclusions Sequential administration of pemetrexed followed by docetaxel may provide the greatest anti-tumor effects for this combination in the treatment of lung cancer.

Keywords Pemetrexed · Docetaxel · Isobologram · Lung cancer

Y. Kano (✉) · M. Tanaka · M. Akutsu
Division of Hematology,
Tochigi Cancer Center, Yonan,
Utsunomiya, Tochigi 320-0834, Japan
e-mail: ykano@tcc.pref.tochigi.jp

K. Mori
Division of Thoracic Diseases,
Tochigi Cancer Center, Utsunomiya,
Tochigi 320-0834, Japan

Y. Yazawa
Division of Orthopedic Oncology,
Tochigi Cancer Center, Utsunomiya,
Tochigi 320-0834, Japan

H. Mano
Division of Functional Genomics,
Jichi Medical University,
Tochigi 329-0431, Japan

Y. Furukawa
Division of Stem Cell Regulation,
Jichi Medical University,
Tochigi 329-0431, Japan

Introduction

Lung cancer is the leading cause of cancer mortality in industrialized countries, with non-small cell lung cancer (NSCLC) accounting for nearly 80% [1]. Although surgery may be curative in early-stage NSCLC, most patients present with inoperable advanced disease. These patients managed with best supportive care alone have a median survival time of only 5 months and a 1-year survival rate of approximately 10% [2]. First-line treatment for patients with advanced NSCLC includes platinum compounds combined with vinorelbine, gemcitabine, or taxanes [3]. This is associated with improved quality of life, but only moderate survival advantages when compared with best supportive

care alone. Therefore, there is an emergent need for effective second-line treatments for NSCLC patients who experience disease progression after first-line chemotherapy. Currently, erlotinib, docetaxel, and pemetrexed are approved as second-line drugs by the US Food and Drug Administration for patients whose tumors have progressed after platinum-based treatments [4, 5].

Small cell lung cancer (SCLC) accounts for approximately 12% of all lung cancers [6]. Compared with NCSLC, SCLC has a rapid doubling time, and earlier development of wide spread metastasis. SCLC is highly sensitive to initial radiotherapy and chemotherapy. The most commonly used regimens include etoposide, cisplatin, doxorubicin, or cyclophosphamide [7]. For limited-stage patients, chemotherapy associated with thoracic radiation was able to produce a cure rate of 10–20%. In extensive disease, the combinations of these agents yields responses of 50–70%, with 20–30% complete remissions, but most patients die from recurrent diseases. The identification of new agents is critical for further progress in the treatment of SCLC, and the evaluation of a variety of agents including docetaxel and pemetrexed has been underway [8–10].

Pemetrexed is a new antifolate that has significant activity against a broad spectrum of solid tumors including lung cancer [11, 12]. Pemetrexed inhibits multiple enzymes involved in folate metabolism including thymidylate synthase, dihydrofolate reductase, and glycinamide ribonucleotide formyltransferase [13]. Pemetrexed arrests cells mainly in S phase and induces apoptosis against tumor cells [14]. Against lung cancers, pemetrexed is non-inferior to docetaxel, with lower hematologic toxicity, and febrile neutropenia and a similar rate of non-hematologic toxicities [12].

The taxanes, paclitaxel and docetaxel, have significant activity in lung cancer. Both inhibit microtubule dynamics and cause G2/M cell cycle arrest. However, there are several differences between them in the pharmacokinetics and pharmacologic actions [15, 16]. Docetaxel demonstrated greater affinity for the tubulin-binding site, wider cell cycle activity, longer intracellular retention time and higher intracellular concentration in tumor cells, more potent antitumor activity in in vitro and in vivo models, and more potent induction of bcl-2 phosphorylation and apoptosis. Paclitaxel has a non-linear pharmacokinetic behavior, while docetaxel demonstrated linear pharmacokinetics and less schedule dependence than paclitaxel.

The combination of pemetrexed and docetaxel may play a major role in the second-line treatment of lung cancers. The wide range of antitumor activity of these agents, their different cytotoxic mechanisms and different toxicity profiles, and the absence of cross-resistance provide the rationale for combining these agents. Since both pemetrexed and docetaxel are cell cycle-specific, disturbances of the cell cycle produced by one drug may influence the cytotoxic effects of the other. Furthermore the drug schedule may play a significant role in the outcome, and therefore, how the drugs are combined requires careful consideration.

We showed that the ordered treatment of pemetrexed followed by paclitaxel may be synergistic, whereas simultaneous administration was potentially antagonistic in a variety of solid tumor cell lines [17]. What is not clear is whether such schedule dependency will be as important for pemetrexed and docetaxel as for pemetrexed and paclitaxel in the treatment of lung cancers. The present study was aimed at characterizing the cytotoxic effects of various pemetrexed and docetaxel combinations and schedules on three human lung cancer cell lines using the isobologram method of Steel and Peckham [18]. Flow cytometry was performed to understand the molecular basis of the schedule-dependent synergism and antagonism of the pemetrexed and docetaxel combination.

Materials and methods

Cell lines

Three human lung cancer lines, A-549 (lung adenocarcinoma), Lu-99 (giant-cell lung cancer), and SBC-5 (small cell lung cancer) were used. A-549 cells were purchased from the American Type Culture Collection (Rockville, MD). Lu-99 and SBC-5 cells were obtained from Health Science Research Resources Bank (Tokyo). These cells were growing as a monolayer in 75-cm^2 plastic tissue culture flasks containing RPMI1640 medium (Sigma Chemical Co., St Louis, MO) supplemented with 10% heat-inactivated fetal bovine serum (FBS) (Sigma) and antibiotics (penicillin G and streptomycin) in a humidified atmosphere of 95% air/5% CO_2 at 37°C. Under these conditions, the doubling times of these cells were 20–30 h.

Drugs

Pemetrexed and docetaxel were kindly provided by Eli Lilly and Company (Indianapolis, IN) and Sanofi-Aventis K.K. (Tokyo, Japan), respectively. Drugs were dissolved with RPMI1640 and stored at −80°C. Drugs were diluted with RPMI-1640 plus 10% FBS before use.

Cell growth inhibition using combined anti-cancer agents

Growing cells were collected by trypsinization, separated and resuspended to a final concentration of 5.0×10^3 cells/ml in fresh medium containing 10% FBS and antibiotics. Cell suspensions (100 µl) were dispensed into the individual wells of a 96-well tissue culture plate with a lid (Costar, Corning, NY). Each plate had one 8-well control column

containing medium alone and one 8-well control column containing cells but no drug. Eight plates were prepared for each drug combination.

Simultaneous and continuous exposure to pemetrexed and docetaxel

After a 20–24 h incubation for cell attachment, solutions of docetaxel and pemetrexed (50 µl) at different concentrations were added to individual wells in final volumes of 200 µl per wells. The plates were incubated under the same conditions for 120 h.

Simultaneous 24 h exposure to pemetrexed and docetaxel

After cell attachment, solutions of docetaxel and pemetrexed (50 µl) at different concentrations were added to individual wells in final volumes of 200 µl per wells. The plates were also incubated under the same conditions for 24 h. The cells were then washed twice with culture medium, and then fresh medium (200 µl) and antibiotics were added. The cells were cultured again for four additional days in drug-free medium.

Sequential exposure to pemetrexed (24 h) followed by docetaxel (24 h) or vice versa

After cell attachment, medium containing 10% FBS (50 µl) and solutions of docetaxel or pemetrexed (50 µl) at different concentrations were added to individual wells. The plates were then incubated under the same conditions for 24 h. The cells were washed twice and fresh medium was added, followed by the addition of solutions of docetaxel or pemetrexed (50 µl) at different concentrations. The plates were incubated again under the same conditions for 24 h. The cells were then washed twice, and the cells were cultured for three additional days in drug-free medium.

MTT assay

Viable cell growth was determined by 3-(4,5-dimethylthiazol-2-yl)-2,5-diphenyltetrazolium bromide (MTT) assay [19]. For all 4 cell lines examined, we established a linear relation between the MTT assay value and the cell number within the range shown.

Isobologram

The dose–response interactions between pemetrexed and docetaxel were evaluated at the IC_{50} level by the isobologram method of Steel and Peckham (Fig. 1) [18]. The IC_{50} was defined as the concentration of drug that produced 50% cell growth inhibition; i.e. a 50% reduction of absorbance. The theoretical basis of the isobologram method and the procedure for making the isobologram has been described in detail [18, 20, 21]. Based on the dose–response curves of pemetrexed and docetaxel, three isoeffect curves were constructed (Fig. 1). If the agents act additively by independent mechanisms, combined data points would lie near the Mode I line (hetero-addition). If the agents act additively by similar mechanisms, the combined data points would lie near the Mode II lines (iso-addition) [14, 16, 17].

Since we cannot know in advance whether the combined effects of two agents will be hetero-additive, iso-additive, or an effective intermediate between these extremes, all possibilities should be considered. Thus, when the data points of the drug combination fell within the area surrounded by mode I and/or mode II lines (i.e. within the envelope of additivity), the combination was described as additive.

We used this envelope to evaluate not only the simultaneous exposure combinations of pemetrexed and docetaxel, but also to evaluate the sequential exposure combinations, since the second agent under our experimental conditions could modulate the cytotoxicity of the first agent.

A combination that gives data points to the left of the envelope of additivity (i.e. the combined effect is caused by lower doses of the two agents than is predicted) can confidently be described as supra-additive (synergism). A combination that gives data points to the right of the

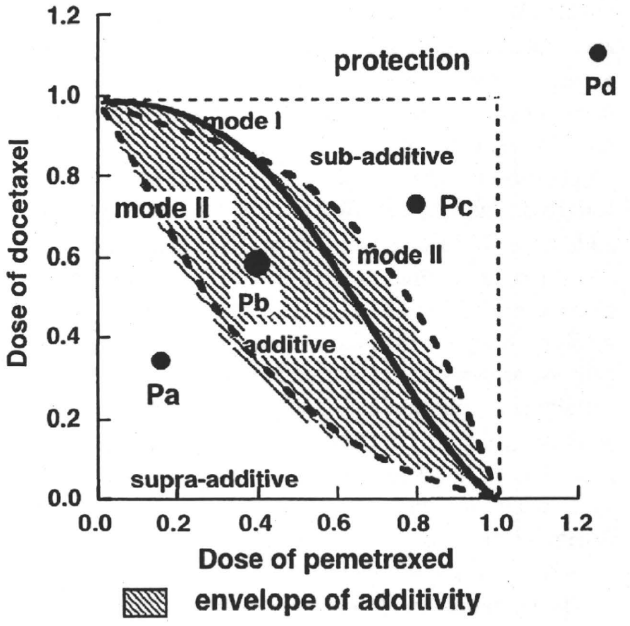

Fig. 1 Schematic representation of an isobologram (Steel and Peckham). The envelope of additivity, surrounded by mode I (*solid line*) and mode II (*dotted lines*) isobologram lines, was constructed from the dose–response curves of pemetrexed alone and docetaxel alone. The concentrations that produced 50% cell growth inhibition were expressed as 1.0 in the ordinate and the abscissa. Combined data points *Pa*, *Pb*, *Pc* and *Pd* show supra-additive, additive, sub-additive, and protective effects, respectively

envelope of additivity, but within the square or on the line of the square can be described as sub-additive (i.e. the combination is superior or equal to a single agent but is less than additive). A combination that gives data points outside the square can be described as protective (i.e. the combination is inferior in cytotoxic action to a single agent). A combination with both sub-additive and/or protective interactions can confidently be described as antagonistic.

Data analysis

Findings were analyzed as described previously [22]. To determine whether the condition of synergism (or antagonism) truly existed, a Wilcoxon signed-rank test was performed to compare the observed data with the predicted minimum (or maximum) data for an additive effect. Probability values (P) ≤ 0.05 were considered significant. Combinations with $P > 0.05$ were regarded as having an additive/synergistic (or additive/antagonistic) effect. All statistical analyses were performed using the Stat View 4.01 software program (Abacus Concepts, Berkeley, CA).

Flow cytometric analysis

SBC-5 cells were treated with 5.0 μM pemetrexed alone, or 1.5 nM docetaxel alone or their combination simultaneously for 24 h. The cells were also treated with pemetrexed for 24 h followed by docetaxel for 24 h or the reverse sequence. The cells were harvested at 72 h and the cell cycle profiles were analyzed by staining intracellular DNA with propidium iodide in preparation for flow cytometry with the FACScan · CellFIT system (Becton-Dickinson, San Jose, CA). The size of the sub-G1, G0/G1 and S+G2/M fractions was calculated as a percentage by analyzing DNA histograms with the ModFitLT 2.0 program (Verity Software, Topsham, ME) [23].

Results

Figure 2 shows the dose–response curves for pemetrexed in A-549, Lu-99, and SBC-5 cells. The dose–response curves were plotted on a semi-log scale as a percentage of the control. The IC_{50} values of pemetrexed against these cells were 1.5 ± 0.4, 0.42 ± 0.10, 1.3 ± 0.2 μM, respectively ($n = 5$). The IC_{50} values of docetaxel against these cells were 1.7 ± 0.2, 1.0 ± 0.1, and 0.82 ± 0.13 nM, respectively ($n = 5$).

The dose–response curves in Fig. 3 show the effect of simultaneous exposure (24 h) (panel a), sequential exposure to pemetrexed followed by docetaxel (panel b), and vice versa (panel c) on the growth of SBC-5 cells. The

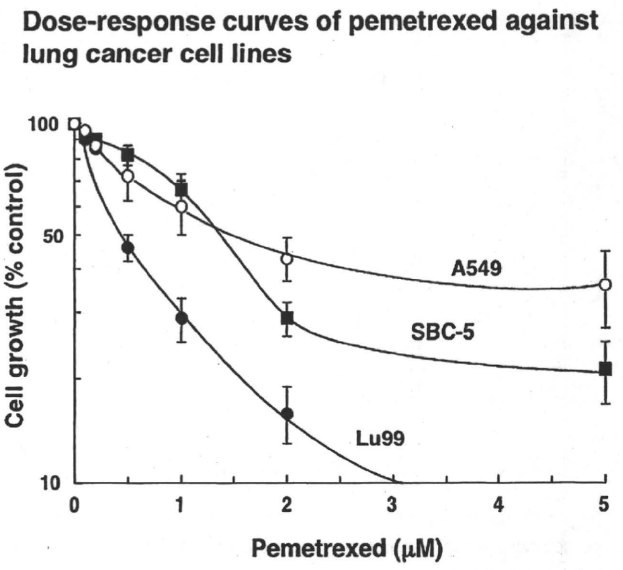

Fig. 2 The dose–response curves of 24 h exposure to pemetrexed against A-549, Lu-99, and SBC-5 cells. Cell growth inhibition was measured using the MTT assay after 5 days and was plotted as a percentage of the control (cells not exposed to drugs). Each point represents the mean ± SEM for at least three independent experiments

pemetrexed concentrations are shown on the abscissa. Dose–response curves in which the docetaxel concentrations are shown on the abscissa are based on the same data (figure not shown). Three isoeffect curves (mode I and mode II lines) were constructed based on the dose–response curves of pemetrexed alone and docetaxel alone. Isobolograms at the IC_{50} level were generated based on these dose–response curves for the combinations.

Simultaneous exposure to docetaxel and pemetrexed for 24 h

Figure 4a shows isobolograms of SBC-5 cells after simultaneous exposure to pemetrexed and docetaxel. The combined data points fell in the areas of subadditivity and protection. The mean values of the observed data (0.71) were larger than those of the predicted maximum values (0.60). The observed data and the predicted maximum data were compared by Wilcoxon signed-rank test. The difference was significant ($P < 0.05$), indicating antagonistic effects (Table 1). Quite similar effects were observed in A-549 and Lu-99 cells (Table 1, isobolograms not shown).

Sequential exposure to pemetrexed for 24 h followed by docetaxel for 24 h

Figure 4b shows isobolograms of SBC-5 cells exposed first to pemetrexed and then to docetaxel. The combined data points fell in the area of supraadditivity. The mean values of the observed data (0.46) were smaller than those

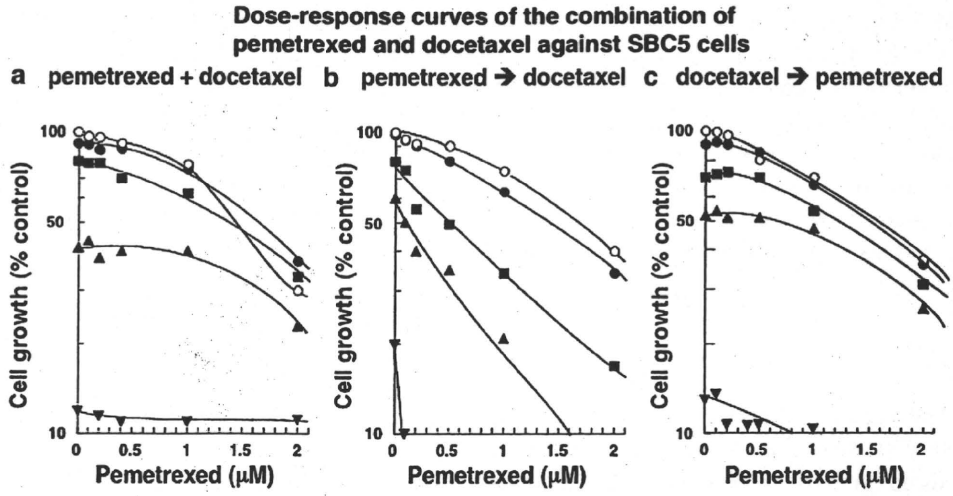

Fig. 3 Schedule dependence of the interaction between docetaxel and pemetrexed in SBC-5 cells. Cells were exposed to these two drugs simultaneously for 24 h (**a**), pemetrexed first for 24 h followed by docetaxel for 24 h (**b**), and vice versa (**c**). The cell number after 5 days was measured using the MTT assay and was plotted as a percentage of the control (cells not exposed to drugs). The concentrations of docetaxel are shown on the abscissa. The concentrations of pemetrexed were 0 (*open circle*), 0.2 (*filled circle*), 0.5 (*filled square*), 1.0 (*filled triangle*) and 2.0 (*filled inverted triangle*) μM, respectively. Data are mean values for three independent experiments; SE was < 25%

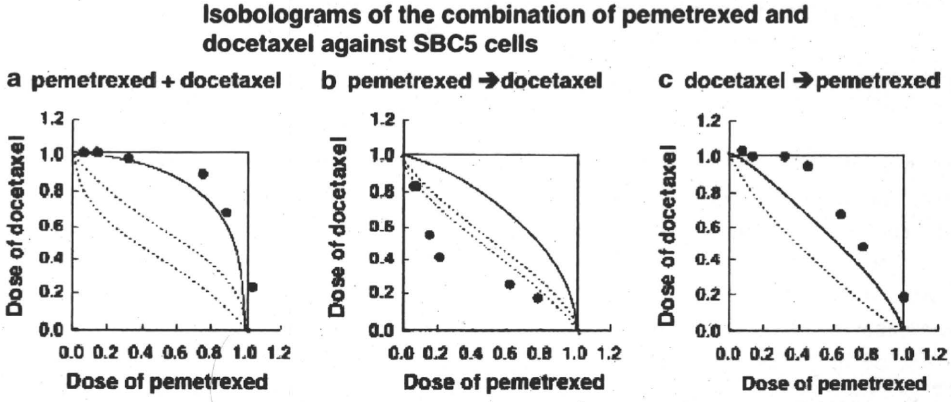

Fig. 4 Isobolograms of simultaneous exposure to docetaxel and pemetrexed for 24 h in SBC-5 cells (**a**). The combined data points fell in the areas of subadditivity and protection. Data are mean values for at least three independent experiments; SE was <25%. Isobolograms of sequential exposure to pemetrexed (24 h) followed by docetaxel (24 h) in SBC-5 cells (**b**). All data points of the combinations fell in the area of supraadditivity. Data are mean values for at least three independent experiments; SE was <20%. Isobolograms of sequential exposure to docetaxel (24 h) followed by pemetrexed (24 h) in SBC-5 cells (**c**). All data points of the combinations fell in the areas of subadditivity and protection. Data are mean values for at least three independent experiments; SE was <25%

of the predicted minimum values (0.60) (Table 1). The difference was significant ($P < 0.05$), indicating synergistic effects. Quite similar effects were observed in Lu-99 cells (Table 1, isobolograms not shown), while additive effects were observed in A-549 cells (Table 1, isobolograms not shown).

Sequential exposure to docetaxel for 24 h followed by pemetrexed for 24 h

Figure 4c shows isobolograms of SBC-5 cells exposed first to docetaxel, followed by pemetrexed. The combined data points mainly fell in the area of subadditivity. The mean values of the observed data were larger than those of the predicted maximum values ($P < 0.02$) (Table 1), indicating antagonistic effects. For A-549 and Lu-99 cells, most combined data points fell within the envelope of additivity and the mean values of the observed data were between those of the predicted minimum and maximum values (Table 1, isobolograms not shown), indicating an additive effect of this schedule.

Simultaneous exposure to pemetrexed and docetaxel for 5 days

For all three cell lines, combined data points fell in the areas of subadditivity and protection, indicating antagonistic effects (Table 1, isobolograms not shown).

Table 1 Mean values of observed data, predicted minimum, and predicted maximum of pemetrexed and docetaxel in combination at IC_{50} level

Schedule	Cell line	n[a]	Observed data	Predicted min.[b]	Predicted max.[c]	Effects
Pemetrexed + docetaxel (24 h)	A-549	8	0.72	0.31	0.55	Antagonism ($P < 0.02$)
	Lu-99	6	>1.0	0.41	0.62	Antagonism ($P < 0.05$)
	SBC-5	6	0.71	0.33	0.60	Antagonism ($P < 0.05$)
Pemetrexed (24 h) → docetaxel (24 h)	A-549	7	0.63	0.31	0.92	Additive
	Lu-99	7	0.29	0.50	0.67	Synergism ($P < 0.02$)
	SBC-5	7	0.46	0.60	0.82	Synergism ($P < 0.02$)
Docetaxel (24 h) → pemetrexed (24 h)	A-549	8	0.64	0.32	0.86	Additive
	Lu-99	8	0.63	0.32	0.85	Additive
	SBC-5	7	0.87	0.36	0.70	Antagonism ($P < 0.02$)
Pemetrexed + docetaxel (5 day)	A-549	6	0.79	0.51	0.68	Antagonism ($P < 0.05$)
	Lu-99	6	0.96	0.45	0.62	Antagonism ($P < 0.05$)
	SBC-5	4	0.73	0.20	0.57	Antagonism ($P < 0.05$)

[a] Number of data points

[b] Predicted minimum value for an additive effect

[c] Predicted maximum value for an additive effect

Cell cycle analysis

The isobologram analysis revealed that pemetrexed and docetaxel had a synergistic effect on two of the three lung cancer cell lines when sequentially administered with pemetrexed first and followed by docetaxel. In contrast, either simultaneous exposure or sequential addition in the reversed order (docetaxel to pemetrexed) resulted in antagonistic or additive effects. We confirmed these results by calculating the size of sub-G1 fractions, which correspond to apoptotic populations, on flow cytometry. As shown in Fig. 5, apoptosis-inducing effects of the two drugs were strongest when cells were exposed to pemetrexed first and followed by docetaxel. In contrast, the cytotoxic effects of docetaxel were significantly suppressed when pemetrexed was added simultaneously or afterward. These data are fully consistent with the results of isobologram analysis.

Cell cycle analysis also provided a clue to understand the mechanisms underlying this observation. Pemetrexed alone induced cell cycle arrest in late G1 to early S phase in SBC-5 cells (see Fig. 6 for representative results, and Table 2 for quantification and statistical analysis of three independent experiments). Docetaxel alone caused the loss of mitotic fractions along with massive apoptosis at a relatively low concentration (1.5 nM). When SBC-5 cells were exposed to both agents simultaneously, the cell cycle pattern was between the patterns of single-agent exposure, and the size of sub-G1 fractions was substantially

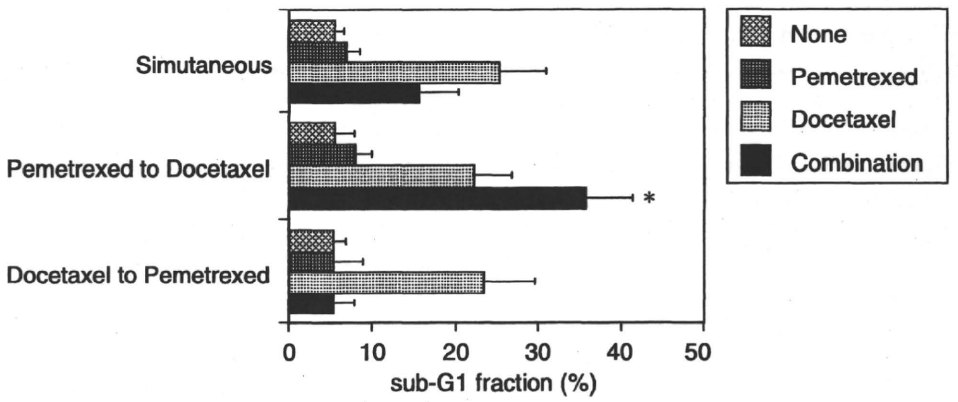

Fig. 5 SBC-5 cells were cultured in the absence (None) or presence of either 5.0 μM pemetrexed (Pemetrexed) or 1.5 nM docetaxel (Docetaxel) alone for 24 h; or in the presence of both drugs for 24 h (Simultaneous); or treated with pemetrexed for 24 h, followed by docetaxel for 24 h (Pemetrexed to Docetaxel); or treated with docetaxel for 24 h, followed by pemetrexed for 24 h (Docetaxel to Pemetrexed). After 72 h, DNA histograms were obtained to calculate the size of sub-G1 fractions as described in "Materials and methods". Data shown are the means ± SD of three independent experiments. The statistical difference was determined by one-way ANOVA with Bonferroni multiple comparison test. An *asterisk* denotes $P < 0.01$

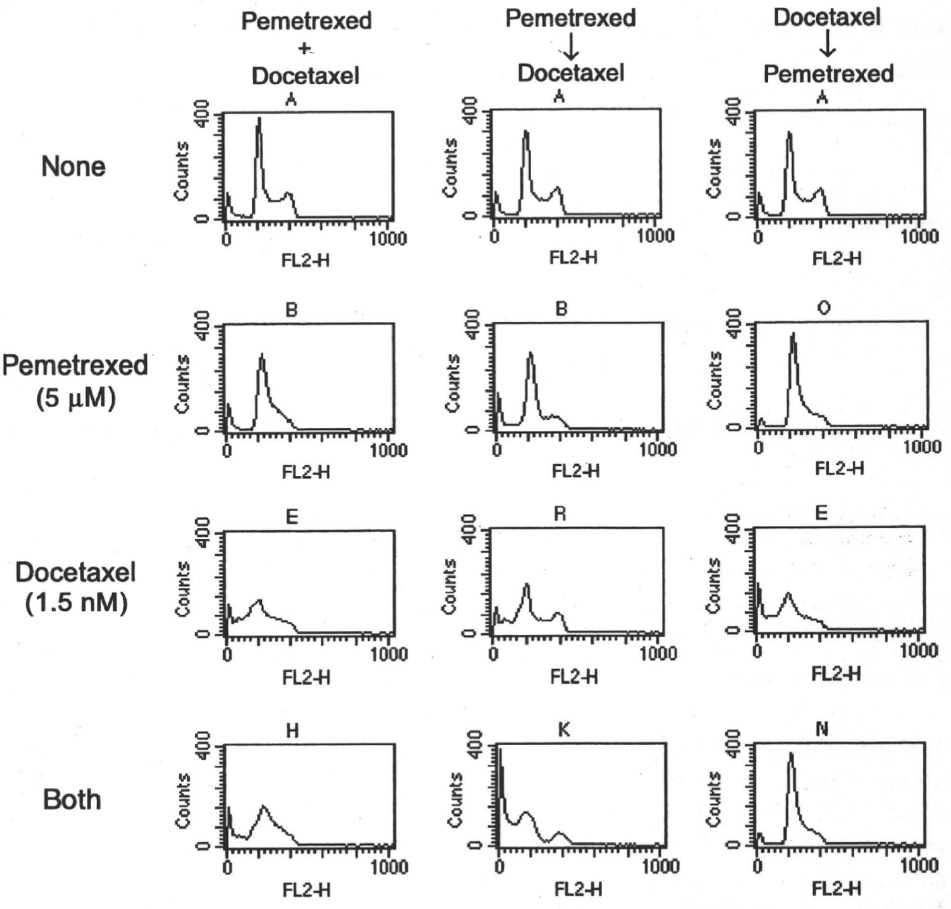

Fig. 6 Cell cycle analysis of SBC-5 cells treated with docetaxel and pemetrexed. *Left column* SBC-5 cells were treated with no drug, 5.0 μM pemetrexed, 1.5 nM docetaxel, or both drug simultaneously for 24 h. *Middle column* SBC-5 cells were treated with 5.0 μM pemetrexed for 24 h, followed by 1.5 nM docetaxel for 24 h. *Right column* SBC-5 cells were treated with 1.5 nM docetaxel for 24 h, followed by 5.0 μM pemetrexed for 24 h. Cells were harvested at 72 h and DNA histogram was obtained as described in "Materials and methods"

reduced. When SBC-5 cells were treated with docetaxel first and followed by pemetrexed, the cell cycle profile was almost identical to that of single exposure to pemetrexed, suggesting that the cell cycle effect of pemetrexed is dominant over that of docetaxel. As a result, the apoptosis-inducing effect of docetaxel was almost completely cancelled in the presence of pemetrexed. In contrast, when SBC-5 cells were treated with pemetrexed first and followed by docetaxel, the proportion of cells in sub-G1 phase was larger than that of cells treated with either pemetrexed or docetaxel alone. This was accompanied by a decrease in S-phase cells. Overall, the results of cell cycle analysis are fully consistent with those of isobologram analysis, and provide the molecular basis of the sequence-dependent differences in cytotoxic interactions between the two agents.

Discussion

In this study, we investigated the effects of pemetrexed in combination with docetaxel on lung cancer cell lines to determine the optimal schedule for this combination. Analysis of the drug–drug interaction effects was carried out using the isobologram method of Steel and Peckham [18], which provides a fundamental basis for assessing whether cytotoxicity induced by combinations of anticancer agents is greater, equal to, or smaller than would have been expected for the individual agents.

We demonstrated that a cytotoxic interaction between pemetrexed and docetaxel is schedule-dependent. Simultaneous exposure to pemetrexed and docetaxel for 24 h and 5 days showed antagonistic effects in all cell lines studied. Sequential exposure to pemetrexed for 24 h followed by docetaxel for 24 h showed synergistic effects in Lu-99 and SBC-5 cells, while it showed additive effects in A-549 cells. Sequential exposure to docetaxel followed by pemetrexed showed additive effects in A-549 and Lu-99 cells, but antagonistic effects in SBC-5 cells. We also used SW620 colon cancer cells for the study, and the combined effects for these schedules were quite the same as those of SBC-5 cells (data not shown).

These findings suggest that the sequential administration of pemetrexed followed by docetaxel may be more cytotoxic to cancer cells and optimal for this combination, while the simultaneous administration of pemetrexed and docetaxel may be less cytotoxic and suboptimal. It should be noted that the sequential administration of pemetrexed

Table 2 Effects of pemetrexed and docetaxel on cell cycle distribution of SBC-5 cells

Schedule	Pemetrexed + Docetaxel (%)	Pemetrexed ↓ Docetaxel (%)	Docetaxel ↓ Pemetrexed (%)
None			
Sub-G1	5.4	4.7	4.7
G1	48.4	51.3	51.3
S	24.9	22.3	22.3
G2/M	21.3	21.7	21.7
Pemetrexed (5 μM)			
Sub-G1	5.5	9.9	2.2
G1	62.8	61.6	68.2
S	28.4	18.1	20.0
G2/M	3.3	10.4	9.6
Docetaxel (1.5 nM)			
Sub-G1	25.2	17.6	21.3
G1	42.8	4.7	50.7
S	27.1	20.0	18.3
G2/M	4.9	17.7	9.7
Both			
Sub-G1	14.6	36.0	2.3
G1	52.1	40.1	66.4
S	22.7	12.2	26.0
G2/M	3.6	11.7	5.3

The proportion of cells in each phase of the cell cycle was calculated with the ModFitLT 2.0 program

followed by docetaxel might be more toxic for normal cells. Since, however, toxicity profiles of both agents are different, increasing overlapping toxicity would likely be mild.

Previously, we evaluated the cytotoxic effects of pemetrexed in combination with paclitaxel in vitro using A-549 cells, breast cancer MCF7, ovarian cancer PA1, and colon cancer WiDr cells in vitro [17]. The results were similar to those of the present study. Although slight differences are present, this would be due to the very strict definitions of synergism and antagonism in the isobologram method (Steel and Peckham). Our previous and present findings suggest that the simultaneous administration of pemetrexed and taxanes is less cytotoxic than the sequential administration of pemetrexed followed by taxanes, and latter schedule should be assessed in clinical trials for the treatment of lung cancer and other solid tumors.

In general, it is difficult to clarify the mechanisms underlying the cytotoxic effects of drug combinations. In this study, however, cell cycle analysis provided a clue to the molecular basis of schedule-dependent synergism and antagonism. The exposure of SBC-5 cells to pemetrexed led to synchronization of most cells that were in late G1 phase to the early S phase of the cell cycle, during which cells are relatively insensitive to docetaxel. This may explain the antagonistic effects of the simultaneous addition of the two agents. In the case of sequential exposure to docetaxel followed by pemetrexed, the cell cycle pattern was almost identical to that of cells treated with pemetrexed alone. This suggests that the cell cycle effect of docetaxel is transient and overcome by the addition of pemetrexed, which results in the abrogation of its cytotoxicity.

In contrast, the sequential exposure to pemetrexed followed by docetaxel produced a striking increase in apoptotic cells along with a decrease in cells in S phase. The effect of docetaxel on S phase cells no longer in pemetrexed-induced cell cycle arrest may cause the synergistic cytotoxicity. The decrease in S phase is compatible with this notion. However, the mechanisms underlying the cytotoxic effects of pemetrexed and docetaxel are still not well understood. The possibility that the drug interactions are due to some unknown mechanism related to complex perturbations of biochemical processes cannot be excluded.

In conclusion, our data show that the antitumor activity of pemetrexed and docetaxel is schedule-dependent. Sequential exposure to pemetrexed followed by docetaxel tended to produce synergistic effects, and would therefore be a suitable schedule, whereas simultaneous exposure to the two agents had antagonistic effects, and may be suboptimal. However, the question of how far these results can be applied in the treatment of patients remains unanswered. Further clinical studies are necessary to clarify whether the therapy sequence alters the antitumor effect and the toxicity of this combination. Our findings provide preclinical rationale for a novel, mechanism-based, therapeutic strategy to be tested in lung cancer patients.

Acknowledgment This work was supported in part by a Grant for Third-Term-Comprehensive Control Research for Cancer from the in-Aid for Cancer Research from the Ministry of Health and Welfare of Japan.

Conflict of interest statement None.

References

1. Shepherd FA (2000) Chemotherapy for advanced non-small-cell lung cancer: modest progress, many choices. J Clin Oncol 18(21 Suppl):35S–38S
2. Non-Small Cell Lung Cancer Collaborative Group (1995) Chemotherapy in non-small cell lung cancer: a meta analysis using updated data on individual patients from 52 randomized trials. Br J Cancer 311:899–909
3. Shepherd FA, Carney DN (2000) Treatment of non-small cell lung cancer: chemotherapy. In: Hansen HH (ed) Textbook of lung cancer. Martin Dunitz, London, pp 213–242
4. Cullen M (2006) Second-line treatment options in advanced non-small cell lung cancer: current status. Semin Oncol 33(1 Suppl 1):S3–S8

5. Massarelli E, Herbst RS (2006) Use of novel second-line targeted therapies in non-small cell lung cancer. Semin Oncol 33(1 Suppl 1):S9–S16
6. Govindan R, Page N, Morgensztern D et al (2006) Changing epidemiology of small-cell lung cancer in the United States over the last 30 years: analysis of the surveillance, epidemiologic, and end results database. J Clin Oncol 24:4539–4544
7. Rosti G, Carminati O, Monti M et al (2006) Chemotherapy advances in small cell lung cancer. Ann Oncol Suppl 5:99–102
8. Socinski MA, Weissman CH, Hart LL et al (2005) A randomized phase II trial of pametrexed (P) plus cisplatin (cis) or carboplatin (carbo) in extensive stage small cell lung cancer (ES-SCLC). Proc ASCO (a 7165)
9. Gronberg BH, Bremnes RM, Aasebo U et al, on behalf of the Norwegian Lung Cancer Study Group (2008) A prospective phase II study: High-dose pemetrexed as second-line chemotherapy in small-cell lung cancer. Lung Cancer Jun 5 [Epub ahead of print]
10. Khan RA, Hahn B (2008) Phase II trial of weekly topotecan with docetaxel in recurrent small cell lung cancer. Proc ASCO (a19111)
11. Adjei AA (2004) Pemetrexed (ALIMTA), a novel multitargeted antineoplastic agent. Clin Cancer Res 10:4276S–4280S
12. Hanna N, Shepherd FA, Fossella FV et al (2004) Randomized phase III trial of pemetrexed versus docetaxel in patients with non-small-cell lung cancer previously treated with chemotherapy. J Clin Oncol 22:1589–1597
13. Shih C, Chen VJ, Gossett LS et al (1997) LY231514, a pyrrolo[2, 3-d]pyrimidine-based antifolate that inhibits multiple folate-requiring enzymes. Cancer Res 57:1116–1123
14. Tonkinson JL, Marder P, Andis SL et al (1997) Cell cycle effects of antifolate antimetabolites: implications for cytotoxicity and cytostasis. Cancer Chemother Pharmacol 39:521–531
15. Jones SE, Erban J, Overmoyer B et al (2005) Randomized phase III study of docetaxel compared with paclitaxel in metastatic breast cancer. J Clin Oncol 23:5542–5551
16. Gligorov J, Lotz JP (2004) Preclinical pharmacology of the taxanes: implications of the differences. Oncologist 9(Suppl 2):3–8
17. Kano Y, Akutsu M, Tsunoda S et al (2004) Schedule-dependent synergism and antagonism between pemetrexed and paclitaxel in human carcinoma cell lines in vitro. Cancer Chemother Pharmacol 54:505–513
18. Steel GG, Peckham MJ (1979) Exploitable mechanisms in combined radiotherapy-chemotherapy: the concept of additivity. Int J Radiat Oncol Biol Phys 5:85–91
19. Kano Y, Sakamoto S, Kasahara T et al (1991) In vitro effects of amsacrine in combination with other anticancer agents. Leukemia Res 15:1059–1064
20. Kano Y, Ohnuma T, Okano T et al (1988) Effects of vincristine in combination with methotrexate and other antitumor agents in human acute lymphoblastic leukemia cells in culture. Cancer Res 48:351–356
21. Kano Y, Suzuki K, Akutsu M et al (1992) Effects of CPT-11 in combination with other anticancer agents in culture. Int J Cancer 50:604–610
22. Kano Y, Akutsu M, Tsunoda S et al (1994) In vitro schedule-dependent interaction between and SN-38 (the active metabolite of irinotecan) in human carcinoma cell lines. Cancer Chemother Pharmacol 42:91–98
23. Kikuchi J, Shimizu R, Wada T et al (2007) E2F–6 suppresses growth-associated apoptosis of human hematopoietic progenitor cells by counteracting proapoptotic activity of E2F–1. Stem Cells 25:2439–2447

ANTICANCER RESEARCH 29: 4589-4596 (2009)

The Cytotoxic Effects of Gemtuzumab Ozogamicin (Mylotarg) in Combination with Conventional Antileukemic Agents by Isobologram Analysis *In Vitro*

MASARU TANAKA[1], YASUHIKO KANO[1], MIYUKI AKUTSU[1], SABURO TSUNODA[1], TOHRU IZUMI[1], YASUO YAZAWA[2], SHUICH MIYAWAKI[3], HIROYUKI MANO[4] and YUSUKE FURUKAWA[5]

Divisions of [1]Hematology and [2]Orthopedic Oncology, Tochigi Cancer Center, Tochigi; [3]Leukemia Research Center, Saiseikai Maebashi Hospital, Gunma; Divisions of [4]Functional Genomics and [5]Stem Cell Regulation, Center for Molecular Medicine, Jichi Medical University, Tochigi, Japan

Abstract. *Background: The CD33 antigen is expressed on leukemia cells in most patients with acute myeloid leukemia (AML) and acute promyelocytic leukemia (APL), and in 20% of patients with acute lymphoblastic leukemia (ALL), while it is absent from pluripotent hematopoietic stem cells and nonhematopoietic cells. Gemtuzumab ozogamicin (GO) is an immunoconjugate of an anti-CD33 antibody linked to calicheamicin, which is a potent cytotoxic agent that causes double-strand DNA breaks, resulting in cell death. GO was developed against CD33 antigen-positive leukemias. The aim of this study was to investigate the cytotoxic effects of this agent in combination with conventional antileukemic agents. Materials and Methods: The cytotoxic effects of GO in combination with antileukemic agents were studied against human CD33 antigen-positive leukemia HL-60, U937, TCC-S and NALM20 cells. The leukemia cells were exposed simultaneously to GO and to the other agents for 4 days. Cell growth inhibition was determined using a MTT reduction assay. The isobologram method was used to evaluate the cytotoxic interaction. Results: GO produced synergistic effects with mitoxantrone, additive effects with cytarabine, daunorubicin, idarubicin, doxorubicin, etoposide and 6-mercaptopurine, and antagonistic effects with methotrexate and vincristine. Conclusion: Our findings suggest that the simultaneous administration of GO with most agents studied would be advantageous for antileukemic activity. The simultaneous administration of GO with methotrexate or vincristine would have little cytotoxic effect, and this combination may be inappropriate. These findings may be useful in clinical trials of combination chemotherapy including GO or other monoclonal antibodies linked to calicheamicin.*

Correspondence to: Dr. Yusuke Furukawa, Stem Cell Regulation, Center for Molecular Medicine, Jichi Medical University, 3311-Yakushiji, Shimotsuke, Tochigi, 329-0498, Japan. Tel: +81285587400, Fax: +81285587501, e-mail: furuyu@jichi.ac.jp

Key Words: Gemtuzumab, calicheamicin, isobologram, CD33, leukemia.

Gemtuzumab ozogamicin (GO) is a humanized anti-CD33 antibody conjugated with the cytotoxic antibiotic calicheamicin (1, 2), which is a potent chemotherapeutic agent with a low therapeutic index that requires targeting to tumor cells for clinical use. On binding to target cells, the antibody-antigen complex is internalized into the cells, and hydrolytic release of the toxic calicheamicin moiety occurs, which subsequently causes DNA double-strand breaks that lead to apoptosis (1, 3, 4).

Acute myeloid leukemia (AML) is a major target of GO, since the CD33 antigen is expressed on blast cells in most patients with AML, while it is absent from pluripotent hematopoietic stem cells and nonhematopoietic cells (5-8). In spite of positive expectations, GO only has a moderate antileukemic activity. It produces a complete response (CR) rate of 10-16% of cases, with another 7-15% achieving CR with inadequate platelet recovery in relapsed CD33-positive AML (9-16). The median survival of patients treated with GO alone is less than 6 months. GO in monotherapy at 9 mg/m^2 is complicated by hepatic veno-occlusive disease in 5-10% of patients. Acute promyelocytic leukemia (APL) cells express large amounts of CD33 and GO is also effective as a single agent with relapsed APL, including those cases with very advanced disease (17).

Around 20% of acute lymphoblastic leukemia (ALL) is also observed to express CD33 and is considered as a target of GO (5-8). Preclinical studies have shown that CD33-positive ALL cells are much more sensitive to GO than are AML cells (18). In clinical studies, several cases of relapsed CD33-positive ALL were reported to achieve complete remission following GO administration (19-20).

0250-7005/2009 $2.00+.40

Combination of lower doses of GO with other agents is the next strategy for improving the response and avoiding toxicity, and clinical studies are in progress for fresh and relapsed AML, APL and CD33-positive ALL cases as remission induction and consolidation therapies with other agents with a variety of schedules (15, 16, 21-26). However, to our knowledge, there are no experimental data available about the cytotoxic effects of GO in combination with conventional antileukemic agents. In the present study, we investigated the *in vitro* effects of GO in combination with antileukemia agents against CD33-positive human leukemia cell lines.

Materials and Methods

Cell lines. Experiments were conducted with CD33-positive human acute myeloid leukemias, U937 and HL-60, and Philadelphia chromosome-positive myeloid leukemia TCC-S, and acute lymphoblastic leukemia NALM20 cells. HL-60 and U937 were obtained from Health Science Research Resources Bank (Osaka, Japan). TCC-S was established in our laboratory (27). NALM20 was kindly donated by Yoshinobu, Matsuo, Hayashibara Biochemical Laboratories Inc., Fujisaki Cell Centre (Okayama, Japan). Cells were maintained in 75-cm^3 plastic tissue culture flasks containing RPMI-1640 medium (Sigma, St. Louis, MO, USA) supplemented with 10% heat-inactivated fetal bovine serum (FBS) (Grand Island Biological Co. Grand Island, NY, USA) and antibiotics. The cell cycle times of rapidly growing U937, HL60 and TCC-S cells were around 24 h, while that of slowly growing NALM20 cells was 70-80 h.

Drugs. Anticancer agents used and their sources were: GO (Wyeth Laboratories, Philadelphia, PA, USA), cytarabine (Nihon Shinyaku Co. Ltd., Tokyo, Japan), daunorubicin (Meiji Co. Ltd., Tokyo, Japan), doxorubicin (Meiji Co. Ltd., Tokyo, Japan), idarubicin (Pfizer Japan Inc. Tokyo, Japan), etoposide (Nihon Kayaku Co. Ltd., Tokyo, Japan), 6-mercaptopurine (Takeda Co. Ltd., Tokyo, Japan), vincristine (Shionogi Co. Ltd., Tokyo, Japan), and methotrexate (Wyeth Lederle Japan Ltd., Tokyo, Japan). All drugs were dissolved in RPMI-1640. Appropriate drug concentrations were made by dilution with fresh medium immediately before each experiment.

Inhibition of cell growth by combination of GO and other agents. Two to four leukemia cell lines were used for the each study of GO in combination with other agents. Leukemia cells lines were harvested from the media and resuspended to a final density of 1×10^5 cells/ml for U937, HL-60, and TCC-S cells, and of 5×10^5 cells/ml for NALM20. Cell suspensions (100 μl) were dispensed into individual wells of 96-well tissue culture plates with lids (Falcon, Oxnard, CA, USA). Eight plates were prepared for the testing of each drug combination. Each plate had one 8-well control column containing medium alone and one 8-well control column containing cells but no drugs. Cells were incubated in a humidified atmosphere of 95% air/5% CO_2 at 37°C overnight. Drug solutions of GO and other drugs at different concentrations were then added (50 μl) to 8 wells containing cell suspensions and the plates were then incubated under the same conditions for 4 days for U937, HL-60 and TCC-S cells, and for 8 days for NALM20 cells.

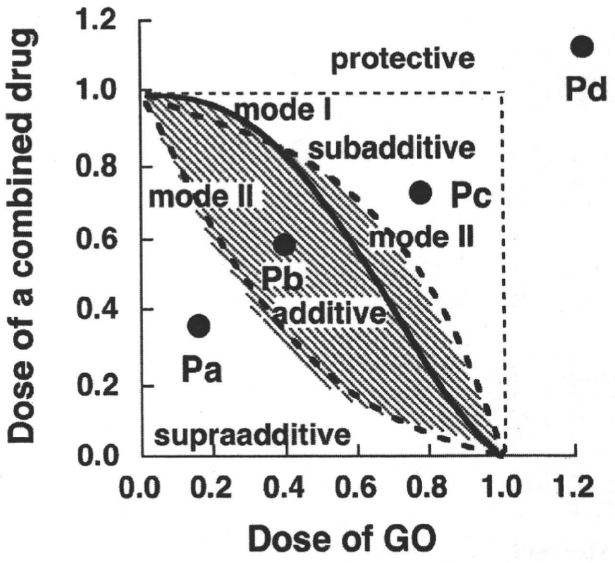

Figure 1. *Schematic representation of isobologram. Envelope of additivity (shaded area), surrounded by mode I (solid line) and mode II (dotted lines) isobologram lines, was constructed from the dose-response curves (shaded area) of GO and a combined drug. The concentrations that produced 80% cell growth inhibition were expressed as 1.0 on the ordinate and the abscissa of the isobolograms. Combined data points Pa, Pb, Pc, and Pd show supraadditive, additive, subadditive, and protective effects, respectively.*

3-(4,5-Dimethylthiazol-2-yl)-2,5-diphenyltetrazolium bromide assay (MTT assay). Viable cell growth was determined using a modified MTT assay as described previously (28).

Isobologram method of Steel and Peckham. Cytotoxic interactions of GO with other agents at the 80% inhibitory concentration (IC_{80}) level were evaluated by the isobologram method of Steel and Peckham (Figure 1) (29). The theoretical basis of the isobologram method and the procedure for making isobolograms have been described in detail previously (30, 31).

Based upon the dose-response curves of GO and the other agents, three isoeffect curves were constructed (Figure 1). If the agents were acting additively by independent mechanisms, the combined data points would lie near the mode I line (hetero-addition). If the agents were acting additively by similar mechanisms, the combined data points would lie near the mode II lines (iso-addition).

Since it is unknown in advance whether the combined effects of two agents will be hetero-additive, iso-additive or an effect intermediate between these extremes, all possibilities should be considered. Thus, when the data points of the drug combination fell within the area surrounded by three lines (envelope of additivity), the combination was regarded as additive. When the data points fell to the left of the envelope, *i.e.* the combined effect was caused by lower doses of the two agents than was predicted, we regarded the drug combination as having a supraadditive effect (synergism). When the points fell to the right of the envelope, *i.e.* the combined effect was caused by higher doses of the two agents than was predicted, but within the square or on the line of the square, we regarded the combination as having a subadditive effect, *i.e.* the combination was

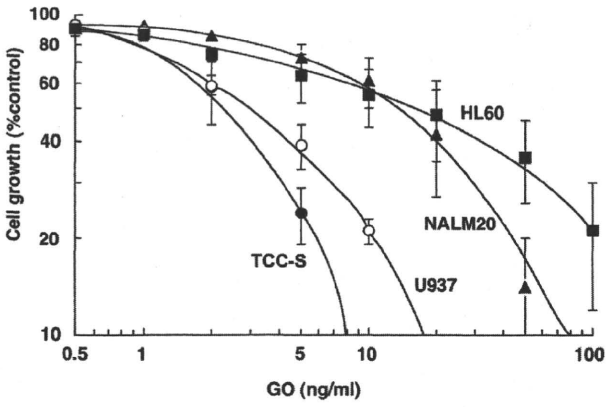

Figure 2. *The dose-response curves of GO in U937, HL-60, TCC-S and NALM20 cells. Cell growth inhibition was measured using the MTT assay and was plotted as a percentage of the control (cells not exposed to drugs). Each point represents the mean±SEM (n>10).*

superior or equal to the single agents but was less than additive. When the data points were outside the square, the combination was regarded as having a protective effect, *i.e.* the combination was inferior in cytotoxic action to the single agents. Bothsubadditive and protective interactions were regarded as antagonism.

Data analysis. To determine whether the condition of synergism (or antagonism) truly existed, statistical analysis was performed. The Wilcoxon signed-ranks test was used for comparing the observed data with the predicted minimum (or maximum) values for additive effects, which were closest to the observed data (*i.e.* the data on the boundary (mode I or mode II lines) between the additive area and supraadditive area (or subadditive and protective areas) (32). Probability (P) values ≤0.05 were considered to be significant. Combinations with $p>0.05$ were regarded as indicating additive/synergistic (or additive/antagonistic) effects. All statistical analyses were performed using the Stat View 4.01 software program (Abacus Concepts, Berkeley, CA, USA).

Results

Figure 2 shows the dose-response curves of GO in U937, HL-60, TCC-S and NALM20 cells. The IC_{80} values of GO alone against U937, HL-60, TCC-S, and NALM20 cells were 10.9±1.1 ng/ml, 100±36 ng/ml, 5.6±1.1 ng/ml, and 41±9 ng/ml, respectively (n>10). Figure 3 shows the dose-response curves for GO in combination with cytarabine, doxorubicin, and vincristine in U937 cells. Each isobologram was generated based on such dose-response curves.

Cytotoxic effects of GO in combination with cytarabine. U937, HL-60 and TCC-S cells were used for this combination study. Figure 4A-C shows the isobolograms of the combination of GO and cytarabine in these cells. In the U937 cells, the combined data points fell within the envelope of additivity (Figure 4A). The mean value of the data (0.55) was larger than that of the predicted minimum value (0.39) and smaller than that of the predicted maximum value for an additive effect (0.74) (Table I), indicating that the simultaneous exposure to GO and cytarabine produced an additive effect. In HL-60 and TCC-S cells, most data points for the combination also fell within the envelope of additivity (Figure 4B, and C). These findings suggest that the simultaneous administration of GO and cytarabine produced additive effects.

Cytotoxic effects of GO in combination with doxorubicin, daunorubicin, idarubicin, or etoposide. Figure 5A-C shows the isobolograms of the combination of GO with doxorubicin in U937, HL-60 and TCC-S cells, respectively. In all cell lines, all combined data points fell within the envelope of additivity, indicating that the simultaneous exposure to GO and doxorubicin produced additive effects (Table I). The simultaneous exposure to GO and daunorubicin, idarubicin, and etoposide showed quite similar effects (isobolograms not shown) in the cell lines studied (Table I)

Cytotoxic interaction between GO and mitoxantrone. U937 and HL60 cells were used for this study and showed similar effects. Most data points for the combination fell in the area of supraadditivity (isobolograms not shown). The mean values of the data were slightly smaller than those of the predicted minimum values for an additive effect (Table I). Statistical analysis showed that the difference was significant, indicating that the simultaneous exposure to GO and mitoxantrone produced marginally synergistic effects.

Cytotoxic effects of GO in combination with 6-mercaptopurine. U937, HL60 and TCC-S cells were used for this study. U937 and TCC-S cells were resistant to 6-mercaptopurine and the cytotoxic effects of this combination were evaluated at the IC_{50} level. In all three cell lines studied, most combined data points fell within the envelope of additivity, indicating that the simultaneous exposure to GO and 6-mercaptopurine produced additive effects (Table I).

Cytotoxic interaction between GO and methotrexate. In all four cell lines studied, most data points for the combination fell in the areas of sub-additivity and protection (isobolograms not shown). The mean values of the observed data were larger than those of the predicted maximum additive values (Table I). The difference was statistically significant, indicating antagonistic effects of the simultaneous exposure to these two agents.

Cytotoxic interaction between GO and vincristine. All four cell lines were used for this study. Figure 6A-C shows the isobolograms of this combination of this combination in U937, HL-60, and TCC-S cells, respectively. In U937, TCC-